DETECTION AND CORRECTION OF GAP MAGNETIC FIELD ERRORS

J.C. Sprott

PLP 1005

July 1987

Plasma Studies

University of Wisconsin

DETECTION AND CORRECTION OF GAP MAGNETIC FIELD ERRORS

J. C. Sprott

I. Introduction

An insulated gap in a current-conducting surface is a potential source of a magnetic field error unless the surface current is led away from the gap by a flange, continuity winding, or the back surface of the conductor in a manner that matches the current density distribution that would exist in the absence of the gap. Common examples are the poloidal and toroidal gaps in the walls and shells that shape the magnetic field in toroidal plasma confinement devices such as multipoles, tokamaks and RFP's. One consequence of such an error is the generation of a normal component of the magnetic field in the gap, whereas the normal component of the field is zero away from the gap to the extent that magnetic field does not soak into the conductor.

Imagine a gap that completely encircles a toroidal shell in either the toroidal (long) or poloidal (short) direction. The normal component of the magnetic field in the gap can be decomposed into its Fourier components as

$$B_n = a_0 + \sum_{m=1}^{\infty} a_m \cos m\theta + b_m \sin m\theta$$

where θ is a periodic variable proportional to the length along the gap and corresponds to a physical angle only in the case of a circularly symmetric gap. Now suppose that a set of N identical coils are placed end-to-end along the gap with each coil covering an angle $2\pi/N$ and measuring the average normal field along its length. The signal in the i^{th} coil is thus given by

$$S_i = \frac{N}{2\pi} \int_{2\pi(i-1)/N}^{2\pi i/N} B_n \, d\theta = a_0 + \sum_{m=1}^{\infty} \alpha_{mi} a_m + \beta_{mi} b_m$$

where

$$\alpha_{mi} = \frac{N}{2\pi m} [\sin 2\pi im/N - \sin 2\pi(i-1)m/N]$$

and

$$\beta_{mi} = \frac{N}{2\pi m} [\cos 2\pi(i-1)m/N - \cos 2\pi im/N]$$

For example, if N=8, the following values of α and β are obtained:

i	α_{1i}	α_{2i}	α_{3i}	α_{4i}	α_{5i}	α_{6i}	α_{7i}	α_{8i}
1	0.900	0.637	0.300	0.000	-0.180	-0.212	-0.129	0.000
2	0.373	-0.637	-0.725	0.000	0.435	0.212	-0.053	0.000
3	-0.373	-0.637	0.725	0.000	-0.435	0.212	0.053	0.000
4	-0.900	0.637	-0.300	0.000	0.180	-0.212	0.129	0.000
5	-0.900	0.637	-0.300	0.000	0.180	-0.212	0.129	0.000
6	-0.373	-0.637	0.725	0.000	-0.435	0.212	0.053	0.000
7	0.373	-0.637	-0.725	0.000	0.435	0.212	-0.053	0.000
8	0.900	0.637	0.300	0.000	-0.180	-0.212	-0.129	0.000

i	β_{1i}	β_{2i}	β_{3i}	β_{4i}	β_{5i}	β_{6i}	β_{7i}	β_{8i}

1	0.373	0.637	0.725	0.637	0.435	0.212	0.053	0.000
2	0.900	0.637	-0.300	-0.637	-0.180	0.212	0.129	0.000
3	0.900	-0.637	-0.300	0.637	-0.180	-0.212	0.129	0.000
4	0.373	-0.637	0.725	-0.637	0.435	-0.212	0.053	0.000
5	-0.373	0.637	-0.725	0.637	-0.435	0.212	-0.053	0.000
6	-0.900	0.637	0.300	-0.637	0.180	0.212	-0.129	0.000
7	-0.900	-0.637	0.300	0.637	0.180	-0.212	-0.129	0.000
8	-0.373	-0.637	-0.725	-0.637	-0.435	-0.212	-0.053	0.000

Note that certain modes (m=8) are completely undetectable with such an arrangement of 8 coils, and other modes (m=4) are measurable only if they have a certain symmetry (odd for m=4). Finally, note that modes above m=4 give signals identical to the low order modes by the process of aliasing. For example, m=5 aliases with m=3, m=6 aliases with m=2, and m=7 aliases with m=1.

With 8 signals, one should be able to determine 8 Fourier coefficients. From the considerations above, the 8 lowest independent coefficients are α_{0i} through α_{3i} and β_{1i} through β_{4i}. The problem then is to invert the matrix of coefficients to derive the Fourier coefficients as follows:

$$a_m = \sum_{i=1}^{N} \alpha'_{mi} S_i \qquad \text{and} \qquad b_m = \sum_{i=1}^{N} \beta'_{mi} S_i$$

The problem can be solved straightforwardly using a modified Gauss-Jordan elimination method with the result:

i	α'_{0i}	β'_{1i}	α'_{1i}	β'_{2i}	α'_{2i}	β'_{3i}	α'_{3i}	β'_{4i}

1	0.125	0.098	0.237	0.196	0.196	0.294	0.122	0.196
2	0.125	0.237	0.098	0.196	-0.196	-0.122	-0.294	-0.196
3	0.125	0.237	-0.098	-0.196	-0.196	-0.122	0.294	0.196
4	0.125	0.098	-0.237	-0.196	0.196	0.294	-0.122	-0.196
5	0.125	-0.098	-0.237	0.196	0.196	-0.294	-0.122	0.196
6	0.125	-0.237	-0.098	0.196	-0.196	0.122	0.294	-0.196
7	0.125	-0.237	0.098	-0.196	-0.196	0.122	-0.294	0.196
8	0.125	-0.098	0.237	-0.196	0.196	-0.294	0.122	-0.196

Note that the analysis here is a generalization of the usual Fourier technique. It is easy to show that in the limit of large N, $\alpha_{mi} = \cos 2\pi im/N$ and $\beta_{mi} = \sin 2\pi mi/N$. Also, for large N, $\alpha'_{mi} = 2\alpha_{mi}/N$ and $\beta'_{mi} = 2\beta_{mi}/N$ except that $\alpha'_{0i} = \alpha_{0i}/N$.

The amplitude and phase of the various modes are given by

$$c_m = [a_m^2 + b_m^2]^{1/2}$$

and

$$\phi_m = \tan^{-1}(b_m/a_m)$$

In terms of c_m and ϕ_m, the normal field at the gap can be written as

$$B_n = c_0 + \sum_{m=1}^{\infty} c_m \cos(m\theta - \phi_m)$$

The error in the wall current density at the gap is given by

$$\Delta J = -\frac{1}{\mu_o r}\frac{\partial B_n}{\partial \theta} = \frac{1}{\mu_o r}\sum_{m=1}^{\infty} m c_m \sin(m\theta - \phi_m)$$

where r is defined such that $2\pi r$ is equal to the length of the gap. Alternately, the error in the wall current density can be estimated directly from the difference between the signals in adjacent coils, ΔS, from

$$\Delta J = -\frac{N\Delta S}{2\pi\mu_o r}$$

II. Example 1: Tokapole II Poloidal Gap

The above ideas have been applied to a measurement of the field errors at the poloidal gap on Tokapole II in the absence of plasma. A set of 8 coils was distributed around the gap as described above. The machine was pulsed at a peak hoop current of 500 kA with a 40:1 turns ratio on the poloidal iron core. The core was biased to reduce the magnetizing current to a negligible (<10kA) value. The measurements were taken 0.5 ms after the field was pulsed at which time the poloidal gap voltage was 80 V. The signals from the coils were not integrated and had approximately the same waveform as the poloidal gap voltage, at least at the times of interest. The coils were numbered sequentially from i=1 at the outer wall top to i=8 at the outer wall bottom and all oriented in the same sense. The data are as follows:

i	S_i
1	-40 mV
2	+50 mV
3	+170 mV
4	-170 mV
5	+170 mV
6	-290 mV
7	-160 mV
8	-90 mV

These measurements imply the following mode spectrum:

m	c_m	ϕ_m
0	0.563	180
1	1.672	103
2	0.422	54
3	2.100	-96
4	1.568	90 (assumed)
	x 10^{-3}	degrees

The amplitudes of the modes are normalized to the total poloidal flux in the machine.

With this normalization, the mode amplitudes must be multiplied by a factor of $NL/\mu_o w = 300$ to get the actual value of B_n/B_t, where L is the inductance of the machine (0.220 μH) and w is the width of the gap (4.78 mm at t=0). Thus the largest mode (m=3) corresponds to about a 60% field error at the radial location of the sense coils. The high order modes fall off rapidly with distance beyond the sense coils, however.

The existence of an m=0 mode implies that there is a net radial flux into the poloidal gap. This flux must return to the machine through the toroidal gap and perhaps through some of the larger portholes. Indeed, a gradient of toroidal gap voltage was measured around the toroidal gap of just the right magnitude to account for the radial flux entering the poloidal gap (to within

the experimental error of ~5%). The field entering the toroidal gap is observed to enter over the entire toroidal circumference of the gap with the largest flux entering at about ± 90° from the poloidal gap. The flux is not symmetrical on the two sides of the poloidal gap, implying a small mutual inductance between the poloidal and toroidal field circuits in vacuum as has been previously observed. Eliminating this coupling between the poloidal and toroidal field circuits is a necessary, but not sufficient, condition for eliminating the m=0 error. The magnitude of the m=0 error is expected to be influenced by the impedance of the toroidal field circuit which was disconnected for these experiments. A measurement of the toroidal gap voltage on either side of the poloidal gap when the poloidal field only is fired provides a sensitive measure of the m=0 component of the poloidal gap error. In the presence of toroidal field and plasma, such a measurement could still be made using a differential amplifier to eliminate the axially symmetric component of the toroidal gap voltage. It is an interesting exercise in topology to show that a coil designed to measure the m=0 component of the poloidal gap error is identical to one designed to measure the n=0 component of the toroidal gap error.

The source of the m=0 error can be easily seen. Imagine an extreme case in which only the top and bottom legs of the core are excited. To supply the required image currents in the inner and outer walls, current most flow around the corners of the vacuum vessel. This is no problem except at the upper outer

corner where the toroidal gap prevents the required current from flowing. Thus all the current for the outer wall must come from the windings on the bottom leg of the core. This leaves the upper leg to supply both the lid and inner wall currents. There is thus a net poloidal current in one direction on one side of the poloidal gap and a corresponding reverse current on the opposite side, producing the m=0 error. The m=0 error should be automatically eliminated when the higher m errors are trimmed to zero, and, indeed, this is observed to be the case.

Note also that a coupling between the poloidal and toroidal gaps can exist even when the m=0 mode is zero. Having no m=0 simply means that there is no net flux leaving the poloidal gap and entering the toroidal gap. There could still be flux lines entering the poloidal gap and leaving the toroidal gap, or vice versa, so long as there is an equal number of lines doing the opposite somewhere along the poloidal gap. In practice, however, it is observed that when the m=0 mode is reduced to a low value, there is very little flux entering or leaving anywhere around the toroidal gap. Conversely, when there is an m=0 component present, the flux tends to have the same sign at all toroidal azimuths around the toroidal gap, although the magnitude may vary.

The m=1 mode is within about 13 degrees of vertical implying that the machine is reasonably up/down symmetric. The sense of the radial field is such as to suggest that some ampere-turns

should be moved from the inside to the outside of the torus. However, the experiment should be repeated with plasma current present.

The m=2 mode would be expected to peak at ±90 degrees if the primary turns were improperly distributed among the four legs of the core. There is clearly a contribution to the m=2 mode from some other source. By running the machine with only two opposite legs of the core driven, a large m=2 mode with amplitude $\sim 10^{-2}$ and within about 5 degrees of ±90 degrees was observed. The magnitude and sign of the m=2 error suggests that the top and bottom legs of the core have about one too many turns and the inner and outer legs have about one too few. Indeed, an error of this magnitude was built into the machine (see PLP 744) in order to permit the legs of the core to be connected in parallel for a 40:1 turns ratio. This error could be corrected by placing a small inductor in series with the top and bottom windings on the core.

The large m=3 mode was unexpected. It is about 180 degrees out of phase with the m=1 component. A number of explanations are possible. The same in/out nonsymmetric error that produces the m=1 can also produce an m=3 component because of its nonsinusoidal nature. The toroidal curvature also produces an m=3 component as does the asymmetric hoop positioning and the asymmetric toroidal gap. Finally, note that the m=3 component is strongly affected by aliasing with the m=5 component. The m=3

error may be reduced by the same steps that reduce the m=1 error, but the extent to which they null under the same conditions remains to be seen.

The m=4 mode is present as would be expected from the fact that the vessel has four-fold symmetry. The error is such as to require a reduction in current in the inner bridges as expected since the inner hoops were moved farther from the wall than the original design case.

To get a better idea of the error in current placement, the quantity ΔJ is plotted versus poloidal angle, measured counter-clockwise from the outer wall midplane. Figure 1 shows the result using the Fourier series and using a direct subtraction of the raw signals from adjacent coils. Note that the Fourier series method, though it gives a smoother curve, introduces additional peaks in ΔJ that are not evidenced in the raw data. The result is to suggest that current should be removed from the inner bridges and added to the inner wall midplane.

An attempt was made to reduce the errors by moving the upper and lower primary windings toward the outside, raising the outer primary slightly, and adding a small inductor (about 6 μH) in series with the top and bottom legs of the core. With a hoop current of 300 kA and a poloidal gap voltage of 38 volts at 0.5 ms, the unintegrated signals from the coils at 0.5 ms without plasma were reduced to the following:

m	c	theta
0	.05625	180
1	.167174	102.888
2	.0421514	54.46233
3	.2100686	-96.42302
4	.1568	90
	percent	degrees

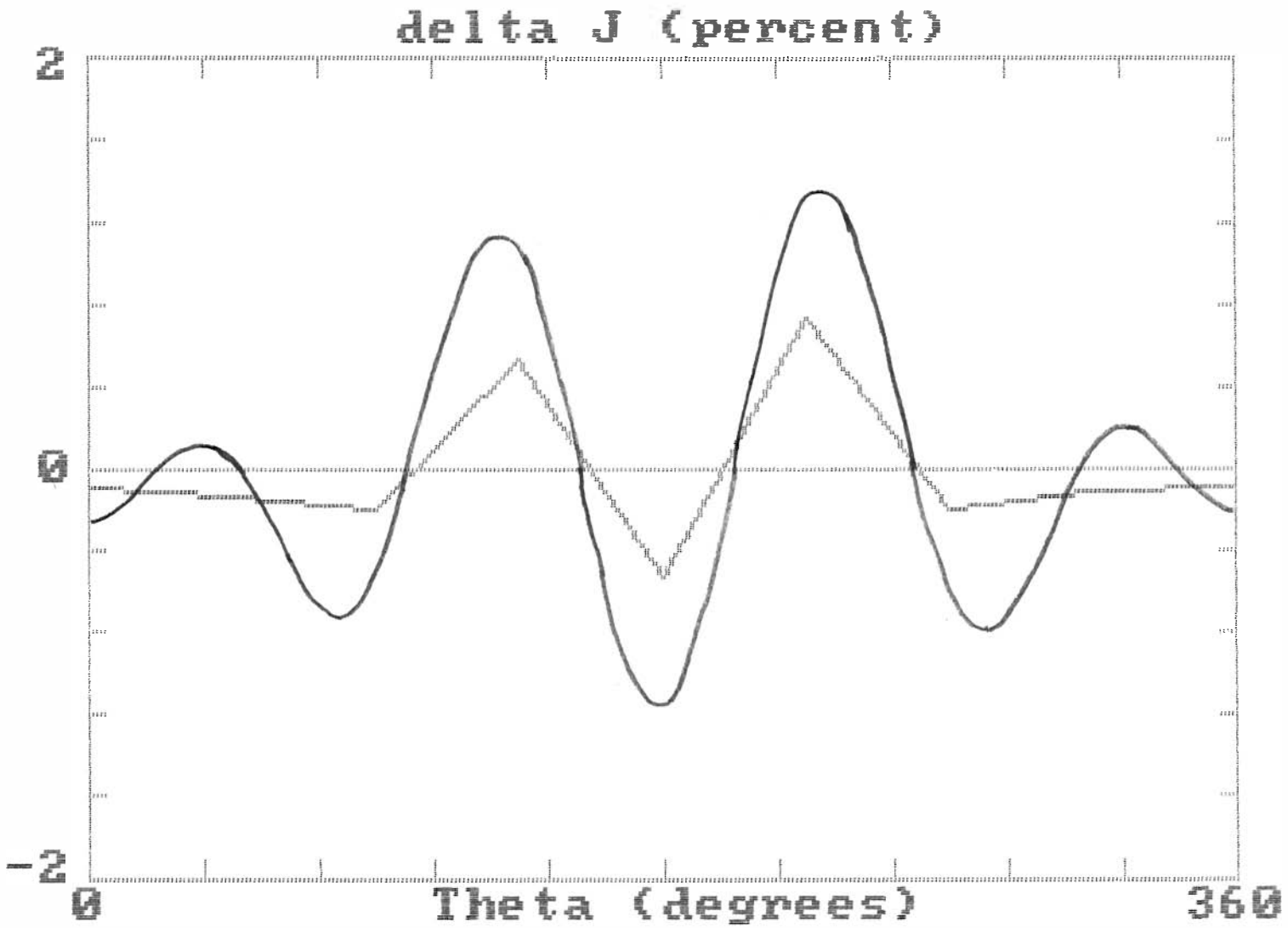

Figure 1. Poloidal gap current error for Tokapole II before correction (t = 0, no plasma).

i	S_i
1	+5 mV
2	-34 mV
3	+13 mV
4	-52 mV
5	+46 mV
6	-8 mV
7	+33 mV
8	-4 mV

As shown in figure 2, the maximum error was reduced about a factor of 2.5. The m=4 error is the dominant one, indicating an excess of current in all bridges and a deficiency in the midplane and midcylinder. The m=0 mode was virtually eliminated, and the m=1, 2 and 3 were reduced by a factor of 3-4.

The relative error has a slight time dependence. After 5 ms, the maximum error has increased slightly, as shown in figure 3, but the general shape and mode composition are the same. A curious feature of the time dependence after the corrections were made is that the integrated signals in coils 2, 4, 5 and 7 follow the waveform of the poloidal field, but the signals in coils 1, 3, 6 and 8 are quite different in shape and on the average smaller by a factor of about 5. These measurements were all taken without plasma. With plasma, the results are qualitatively similar since the plasma current is only about 11% of the hoop

(17)

m	c	theta
0	6.578948E-04	0
1	5.108413E-02	-84.73289
2	1.176181E-02	105.2551
3	5.236061E-02	-81.37469
4	.1021263	90
	percent	degrees

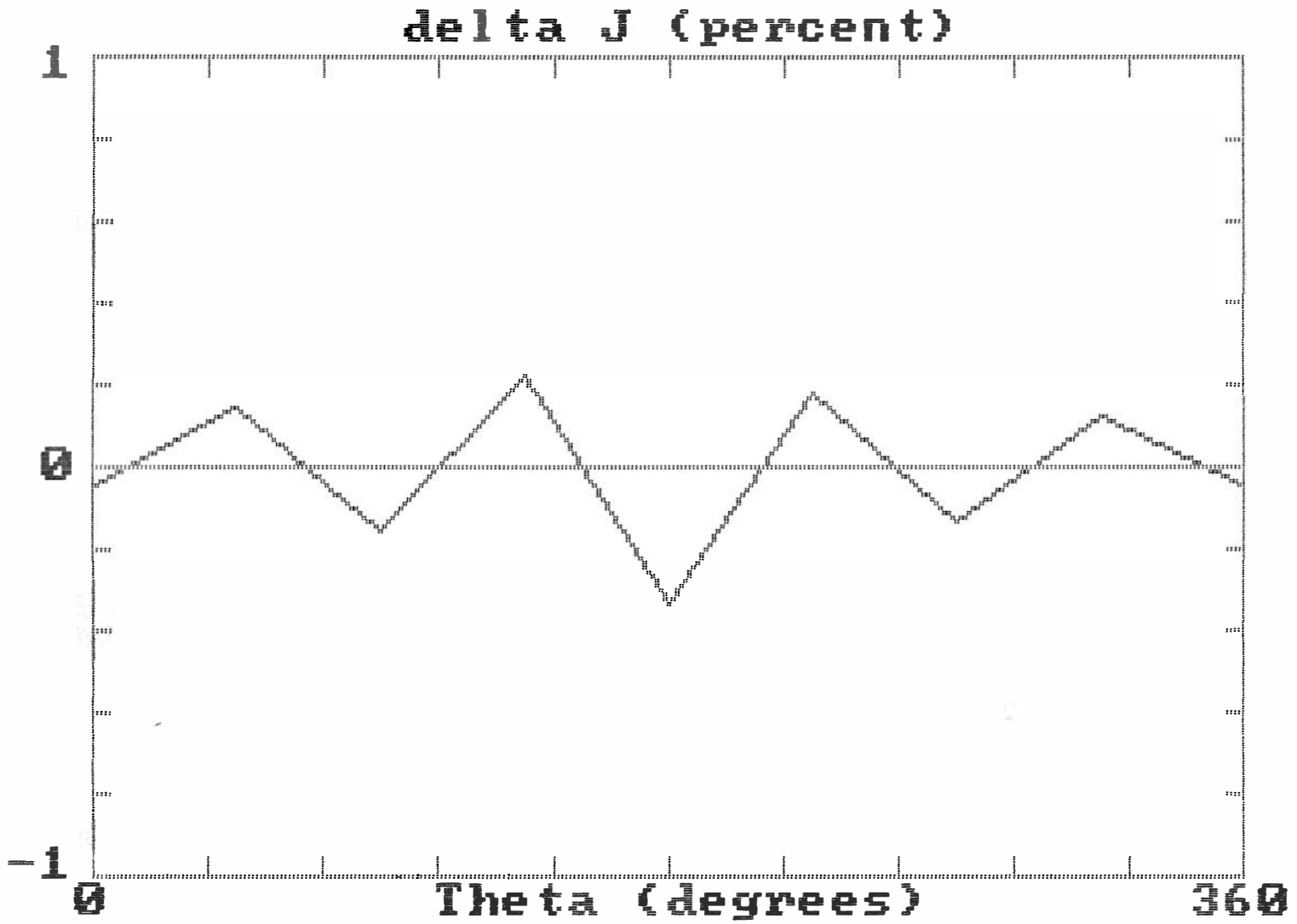

Figure 2. Poloidal gap current error for Tokapole II after correction (t = 0, no plasma).

m	c	theta
0	7.291667E-03	0
1	7.934416E-02	-95.46629
2	1.154941E-02	98.13009
3	.0426235	-87.51241
4	.1355667	90
	percent	degrees

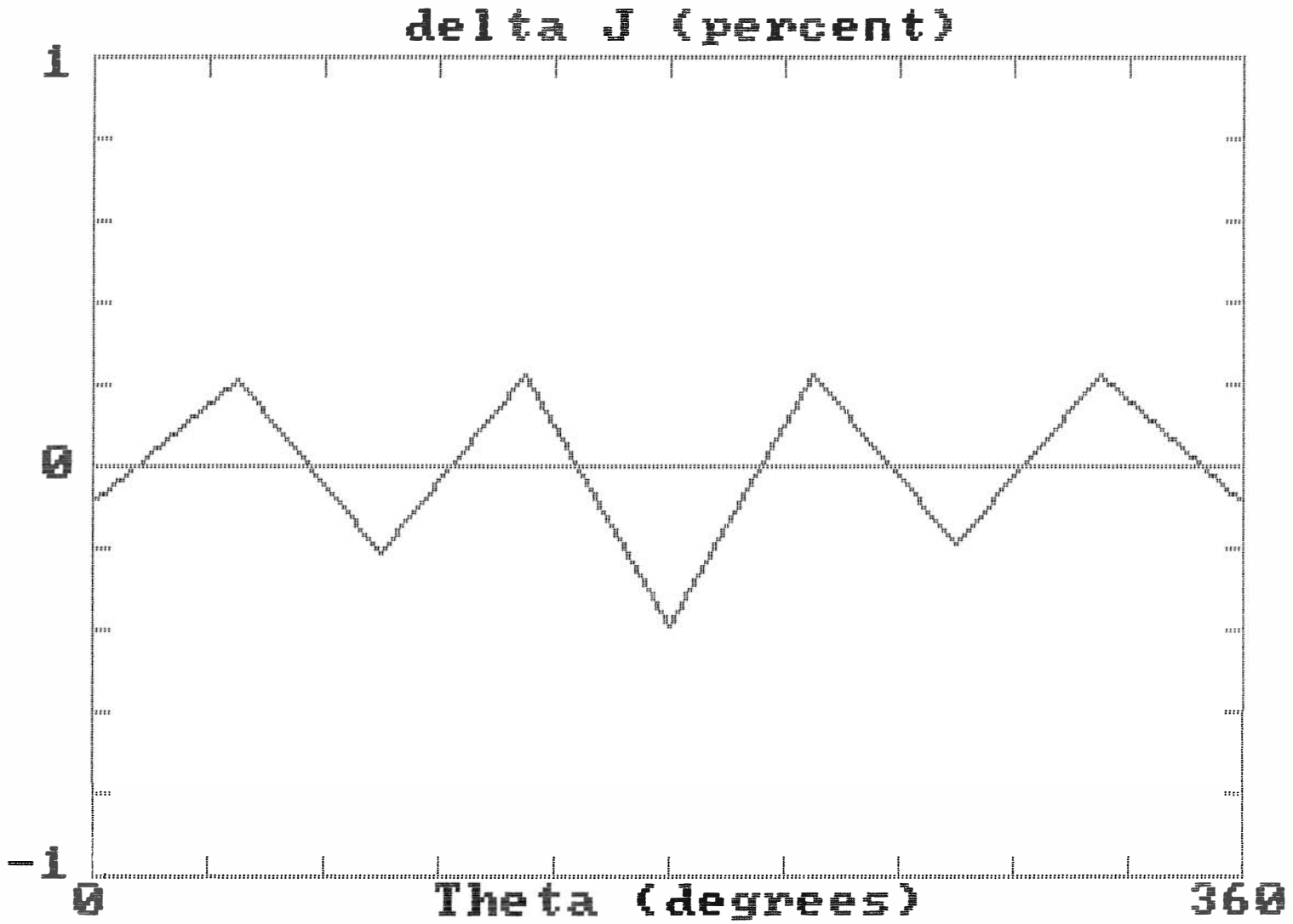

Figure 3. Poloidal gap current error for Tokapole II after correction (t = 5 ms, no plasma).

current.

III. Example 2: Poloidal Divertor RFP Poloidal Gap

The same procedure as above was applied to a measurement of the field errors at the poloidal gap on the poloidal divertor RFP in the absence of plasma. A set of 8 coils was distributed around the gap as described above. The machine was pulsed at a peak hoop current of 250 kA with an 8:1 turns ratio on the poloidal iron core (four winding bundles in parallel). The magnetizing current was negligible. The measurements were taken 1.0 ms after the field was pulsed at which time the poloidal gap voltage was 110 V. The signals from the coils were not integrated and had approximately the same waveform as the poloidal gap voltage, at least at the times of interest. The coils were numbered sequentially from i=1 at the outer wall top to i=8 at the outer wall bottom and all oriented in the same sense. The data are as follows:

i	S_i
1	+125 mV
2	+400 mV
3	-290 mV
4	+650 mV
5	-700 mV
6	+200 mV
7	-500 mV
8	-130 mV

These measurements imply the following mode spectrum:

m	c_m	ϕ_m
0	0.278	180
1	2.315	88
2	0.579	65
3	3.836	89
4	4.428	-90 (assumed)
	x 10^{-3}	degrees

The amplitudes of the modes are normalized to the total poloidal flux in the machine.

With this normalization, the mode amplitudes must be multiplied by a factor of $NL/\mu_o w = 2770$ to get the actual value of B_n/B_t, where L is the inductance of the machine (1.83 μH) and w is the width of the gap (4.20 mm at t=0). Thus the largest mode (m=4) corresponds to about a 1200% field error at the radial location of the sense coils. The high order modes fall off rapidly with distance beyond the sense coils, however.

The relative errors in the RFP are typically 2-3 times larger than the corresponding errors in Tokapole II, especially for the m=4 mode which is large because the turns on the legs of the core are clumped more than desired near the midplane and midcylinder rather than in the bridges.

As for the Tokapole, ΔJ is plotted versus poloidal angle in figure 4. The result indicates the predominance of the m=3 mode but out of phase with the Tokapole case. The implication is that current should be removed from the inner wall midplane and added to the inner bridges. This was done shortly before the machine was decommissioned, and although the error was reduced, the plasma performance was not improved.

The time dependence of the above errors was calculated by Beckstead, and his results are included as figure 5 for the case with no plasma. The mode amplitudes and phases are relatively constant, at least for the first five milliseconds of the pulse, except that the m=2 mode grows slightly. The variation near t=0 is a result of the division of two small numbers since both the error field and the poloidal field start at zero at t=0. The growth of the m=2 mode could be corrected by varying the relative inductance and resistance of the various winding bundles on different legs of the iron core. Some attempts at this were made. More detailed time-dependent measurements of the gap errors in the presence of toroidal field and plasma were made in the last week of operation of the machine by Beckstead, Sarff, Almagri and Assadi, and will be reported elsewhere.

m	c	theta
0	2.784091E-02	180
1	.2314948	87.82032
2	.0578062	65.40988
3	.3835766	88.85519
4	.4427818	-90
	percent	degrees

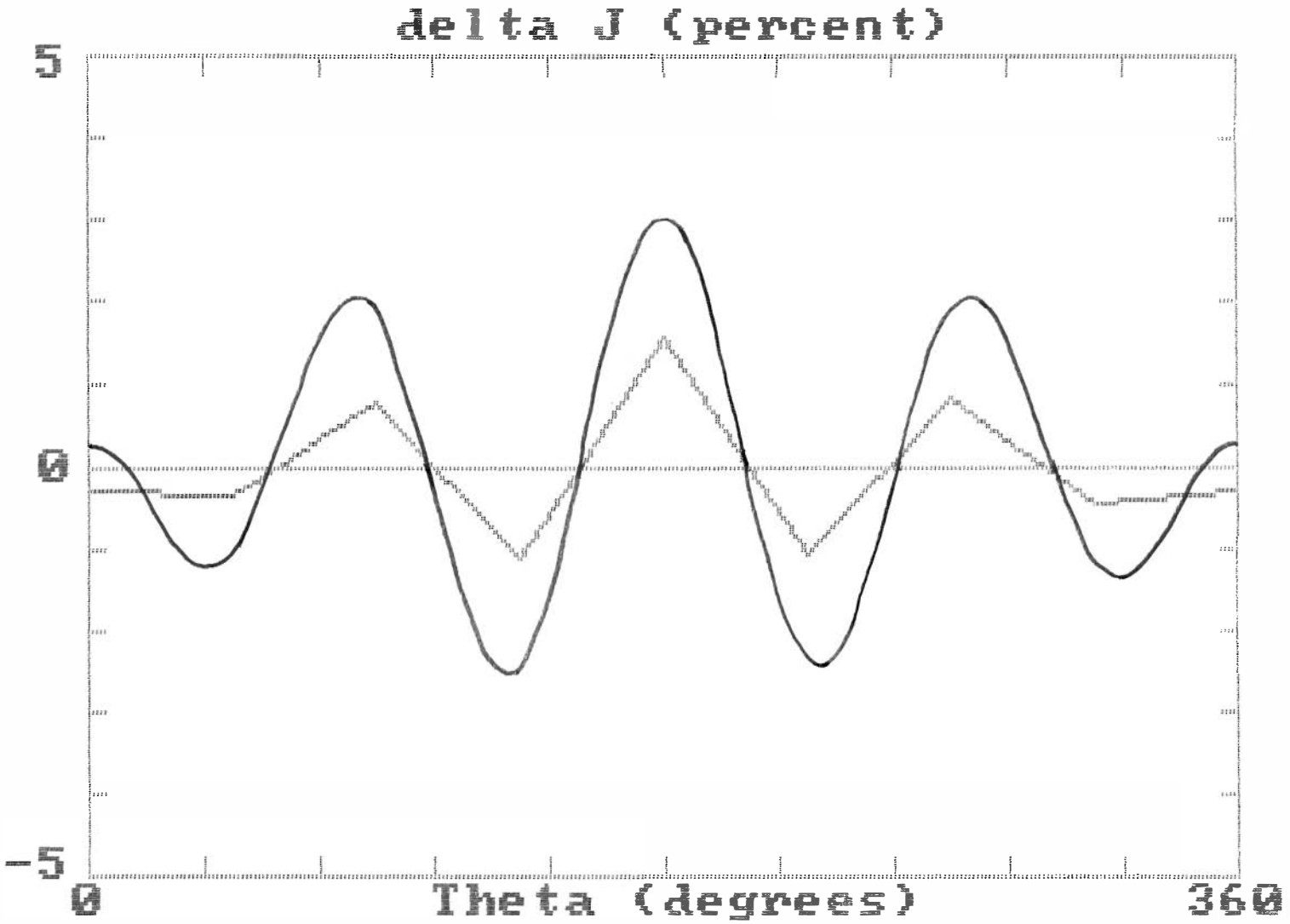

Figure 4. Poloidal gap current error for Poloidal Divertor RFP before correction (t = 0, no plasma).

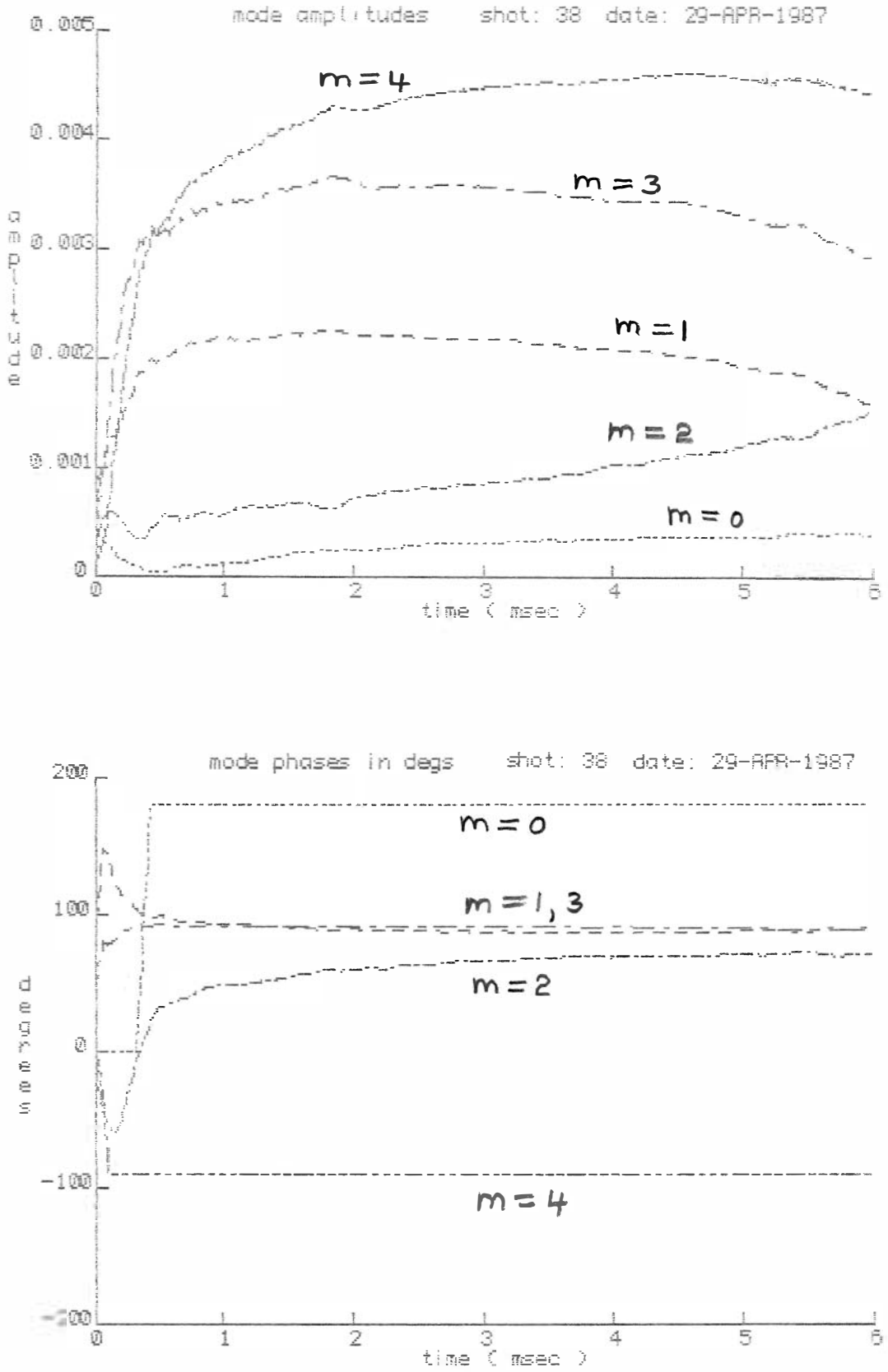

Figure 5. Time-dependence of amplitude and phase of the various modes of the poloidal gap radial field error for Poloidal Divertor RFP (no plasma).

IV. Effect of Gap Errors on the Flux Plot

A field error at any gap in a conductor bounding an axisymmetric magnetic field in a toroid in general destroys the axisymmetry. The result may be a bump in the magnetic flux surfaces, islands in the flux topology, or a region of stochastic wandering of the field lines between two well defined surfaces. If the error is characterized by particular poloidal and toroidal mode numbers, m and n, respectively, islands will form in the vicinity of the surface $q = m/n$ where q is the safety factor, equal to $B_t r/B_p R$ for a large aspect ratio (R/r), circular system. In general, an error is characterized by a broad spectrum of m and n values, causing islands throughout the flux plot with widths proportional to the square root of the amplitude of the component of the error with which they are resonant:

$$\Delta r \approx 4\left[\frac{B_r}{B_p}\,\frac{r}{ndq/dr}\right]^{1/2}$$

The overlapping of these islands when the error is large causes the stochastic wandering of the field lines that is considered to be especially detrimental to plasma confinement.

The normal magnetic field entering or leaving a gap gives rise to an error field throughout the device. The easiest way to model this field is to line the gap with a row of magnetic monopoles, positive where flux enters the gap and negative where it leaves. The monopole strength is precisely what is measured by the sense coils at the gap. The magnetic field can be

calculated from the array of monopoles by superposition in the same way that Coulomb's law is used to calculate the electric field produced by an array of charges, namely

$$\underline{B} = \sum_{i=1}^{N} S_i \underline{r}_i / 4\pi r^3$$

Actually, this procedure is not quite accurate since the field near the gap is unidirectional, whereas the field very near a monopole or point charge is isotropic. This difference is important only near the gap and is not thought to greatly affect the flux plot calculation except perhaps very near the wall. The effect of making this assumption should be to narrow the n-spectrum and to broaden the m-spectrum somewhat.

Using this procedure, eight monopoles were assumed to be located around the rim of the Tokapole poloidal gap, each at the center of one of the sense coils, and with a magnitude proportional to the strength of the flux entering the gap through that coil. Actually, the m=0 component was first subtracted out, although it could also have been included by distributing additional monopoles appropriately along the toroidal gap. Figure 6 shows the resulting magnetomotive force (mmf) surfaces (magnetic scalar potential) in the plane of the gap that results from this approximation. The error field is perpendicular to these surfaces with a magnitude proportional to their density. Near the center of the machine, the predominance of the m=1 (vertical) field is apparent. On the axis of the machine, the error field is calculated to have a value of 5.2 gauss when the

Figure 6. Magnetic scalar potential of error field in the plane of the poloidal gap of Tokapole II before correction (t = 0, no plasma).

total poloidal flux in the machine is 0.066 webers (corresponding to a hoop current of 300 kA).

To estimate the effect of the gap error on the flux plot of Tokapole II, the field error as calculated above was superimposed on the equilibrium field of the hoops as represented by four, straight, current filaments. The filaments were placed at $x = \pm 0.145$ m and $y = \pm 0.145$ m, each carrying a current $I_h/4$. Actually, the electrical centers of the hoops were displaced from their geometric centers along a diagonal by an amount $\delta \approx r_h(v-1)/2(v+1)$, where r_h is the hoop minor radius (0.025 m) and v is the maximum variation of the poloidal field over the surface of the hoop (see PLP 977). Since v depends on the plasma current, δ (in meters) was approximated by

$$\delta = 0.0042(1+5I_p/I_h)$$

The poloidal gap was taken as a square at $x = \pm a$ and $y = \pm a$, where $a = 0.22$ m. The plasma was represented as a toroidal current density distribution proportional to $1/r$ (giving a spatially constant poloidal field strength contribution from the plasma) with a magnitude adjusted to give the desired total plasma current. The toroidal field B_t was taken as constant over the x-y plane. Periodic boundary conditions were applied in the z-direction with a period of $L = 2\pi R_o = 3.14$ m. The poloidal gap was assumed to be at $z = L/2$, and the position of the field line was plotted every time it punctures the x-y plane at z=0.

Even using the simplistic representation of the Tokapole with the gap errors as described above, following several field lines for hundreds of toroidal transits with sufficient accuracy requires large amounts of computer time. The algorithm used was a fourth order Runge-Kutta with a fixed step size of 5 mm. The code solves simultaneously the three equations $dx/d\ell = B_x/B$, $dy/d\ell = B_y/B$ and $dz/d\ell = B_z/B$ where $d\ell$ is an increment of length in the local direction of $\underline{B}$ and $B = [B_x^2 + B_y^2 + B_z^2]^{1/2}$. Initial conditions were taken as y=z=0, and x in ten equal increments between 0 and a. The program as listed in Appendix A was written in Turbo BASIC and run on an IBM PC-XT compatible with an 8087 math coprocessor. Each transit required several minutes of computation, and a whole flux plot required about a day.

First, the code was run in the absence of field errors to ensure that the numerical accuracy was adequate and to produce an equilibrium flux plot. The result as shown in figure 7 for I_h = 300 kA, I_p = 30 kA and B_t = 0.5 tesla, strongly resembles the numerically calculated flux plot for the actual Tokapole. The corresponding q-profile as a function of r/a measured across the midplane is shown in figure 8.

Next, the gap field errors were added with a magnitude corresponding to their value before any improvements were made. The result in figure 9 shows considerable stochasticity outside

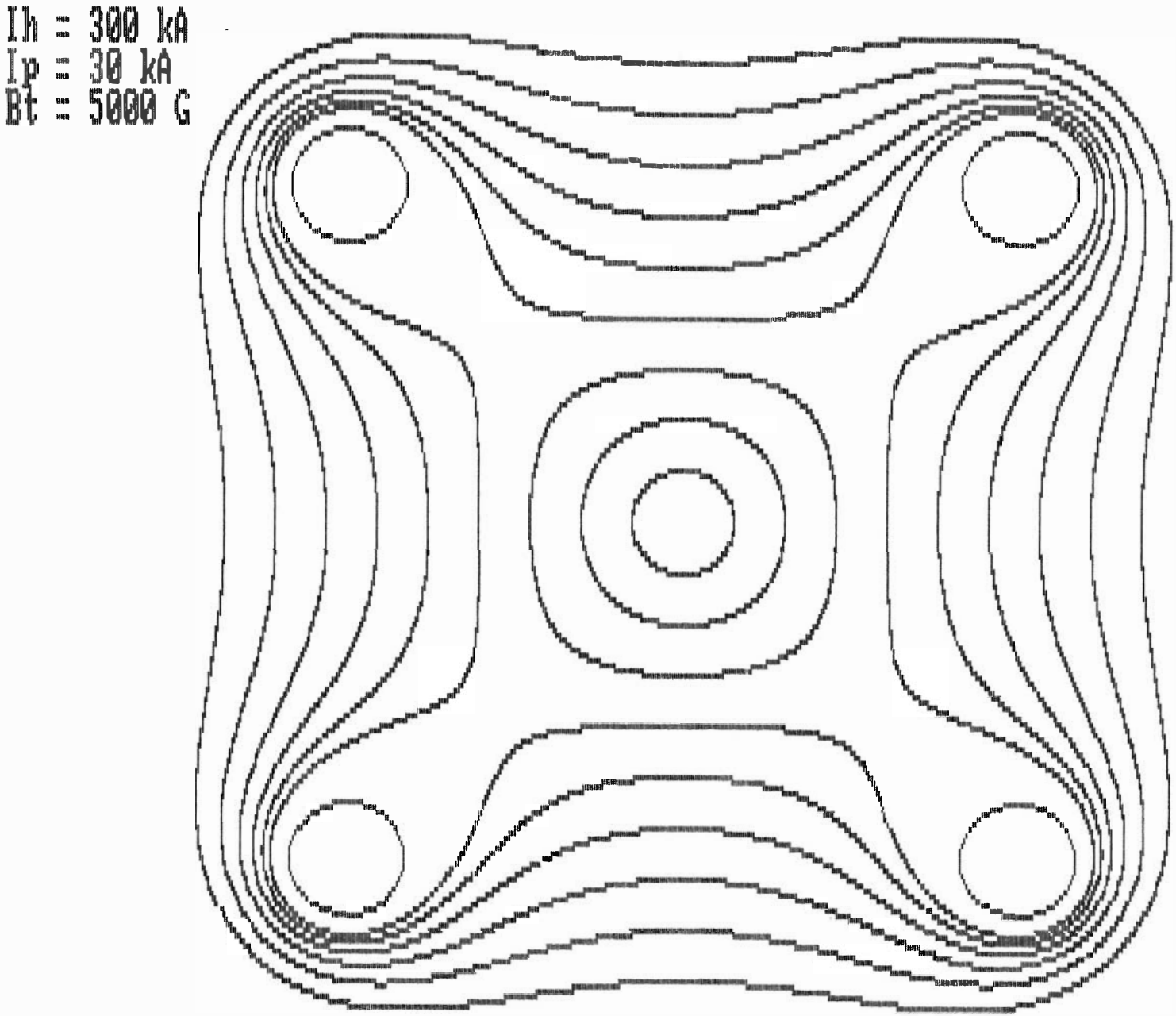

Figure 7. Equilibrium field flux plot used to model Tokapole II (no errors, with plasma).

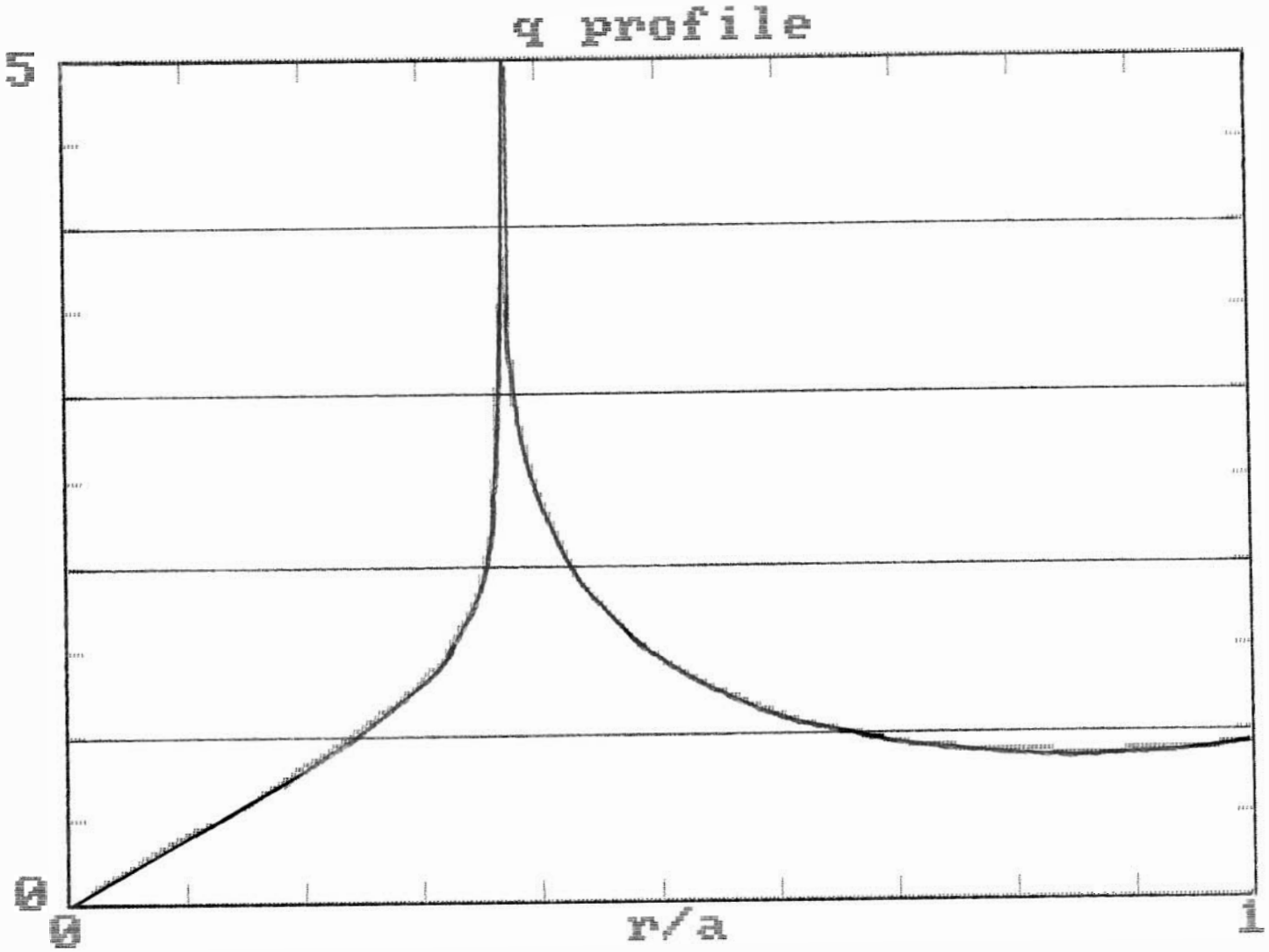

Figure 8. Radial q-profile in the midplane of the flux plot used to model Tokapole II (no errors, with plasma).

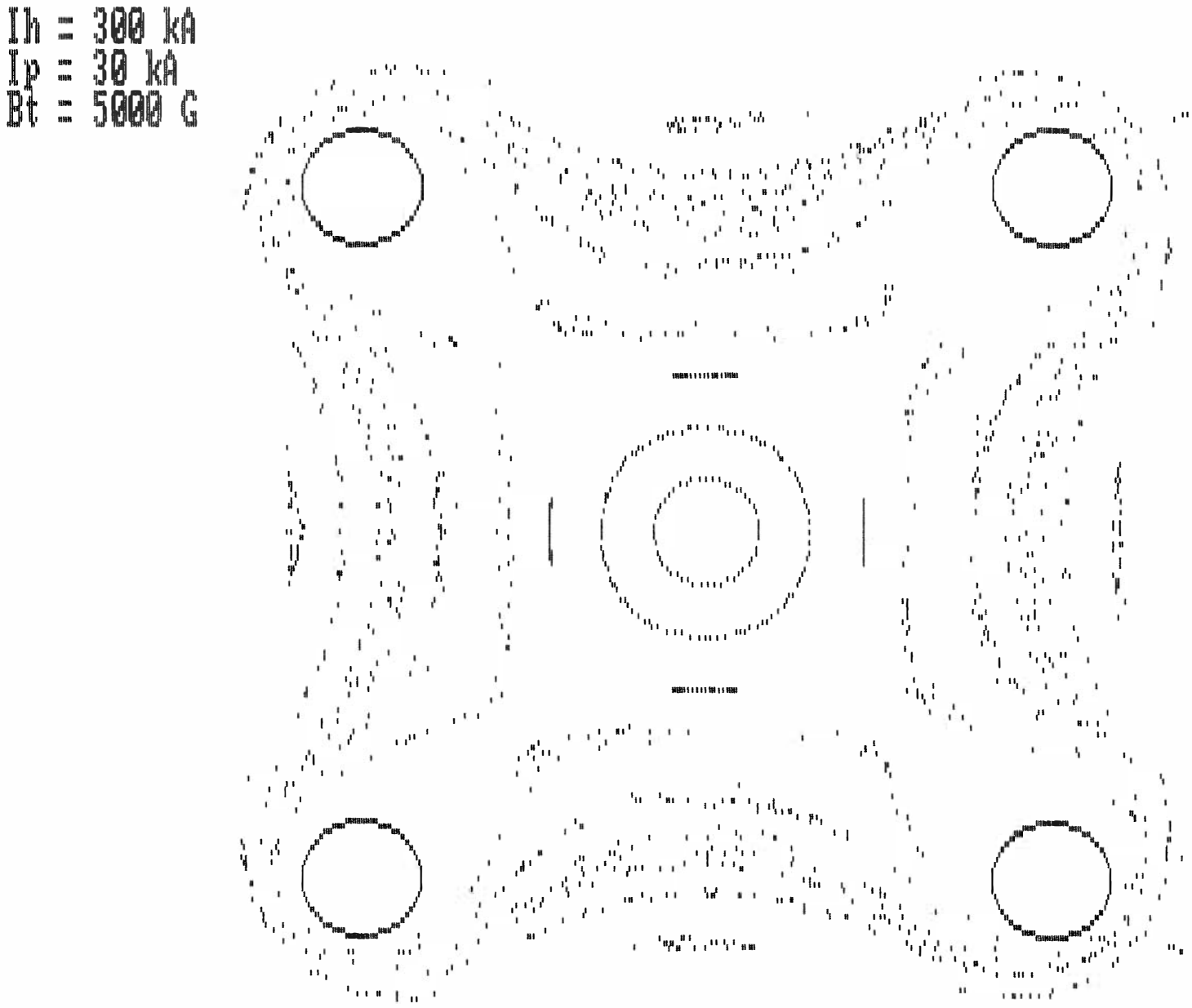

Figure 9. Poloidal puncture plot for Tokapole II before correction (with plasma).

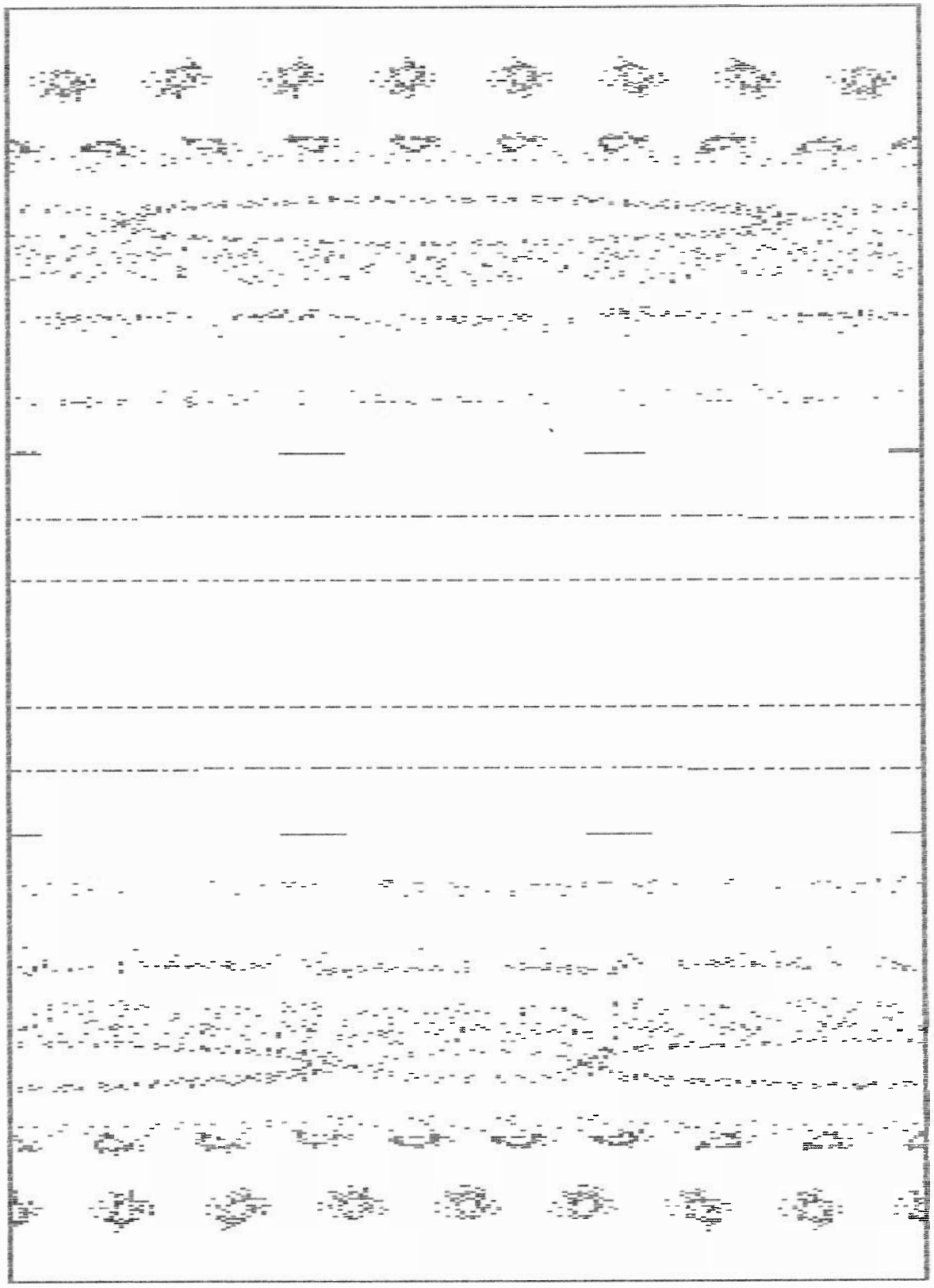

Figure 10. Toroidal puncture plot for Tokapole II before correction (with plasma).

the separatrix. Of course, the q-profile is more strongly sheared than in the real case because of the representation of the plasma such that q goes from 0 to ∞ between the axis and the separatrix. Figure 10 shows the same case, but in the x-z plane for y=0. The stochasticity near the walls is equally evident here.

Figure 11 shows the mmf surfaces in the plane of the gap after the corrections were made. This is the 0.5 ms case without plasma. Applying these errors to an equilibrium Tokapole field with I_h = 300 kA and I_p = 30 kA gives the puncture plots in figures 12 and 13. Some islands and stochasticity are evident but much reduced from the case before the errors were corrected. The design case of I_h = 500 kA, I_p = 100 kA and B_t = 0.5 tesla was also examined with the result as shown in figures 14 and 15. The flux surfaces are not quite as well defined as for the lower-current case.

An attempt was also made to ascertain the quality of the flux surfaces for the poloidal divertor RFP in the presence of the measured gap errors. As with the Tokapole, the device was represented as a cylinder of square cross section with filamentary currents near the corners to represent the hoops. The dimensions chosen were a = 0.5 m and $L = 2\pi R_o$ = 8.73 m. The hoops were placed at x = ±0.32 m and y = ±0.32 m with r_h = 0.021 m, each carrying current $I_h/4$. The fourth order Runge-Kutta scheme used a step size of 1 cm. The equilibrium flux plot (no

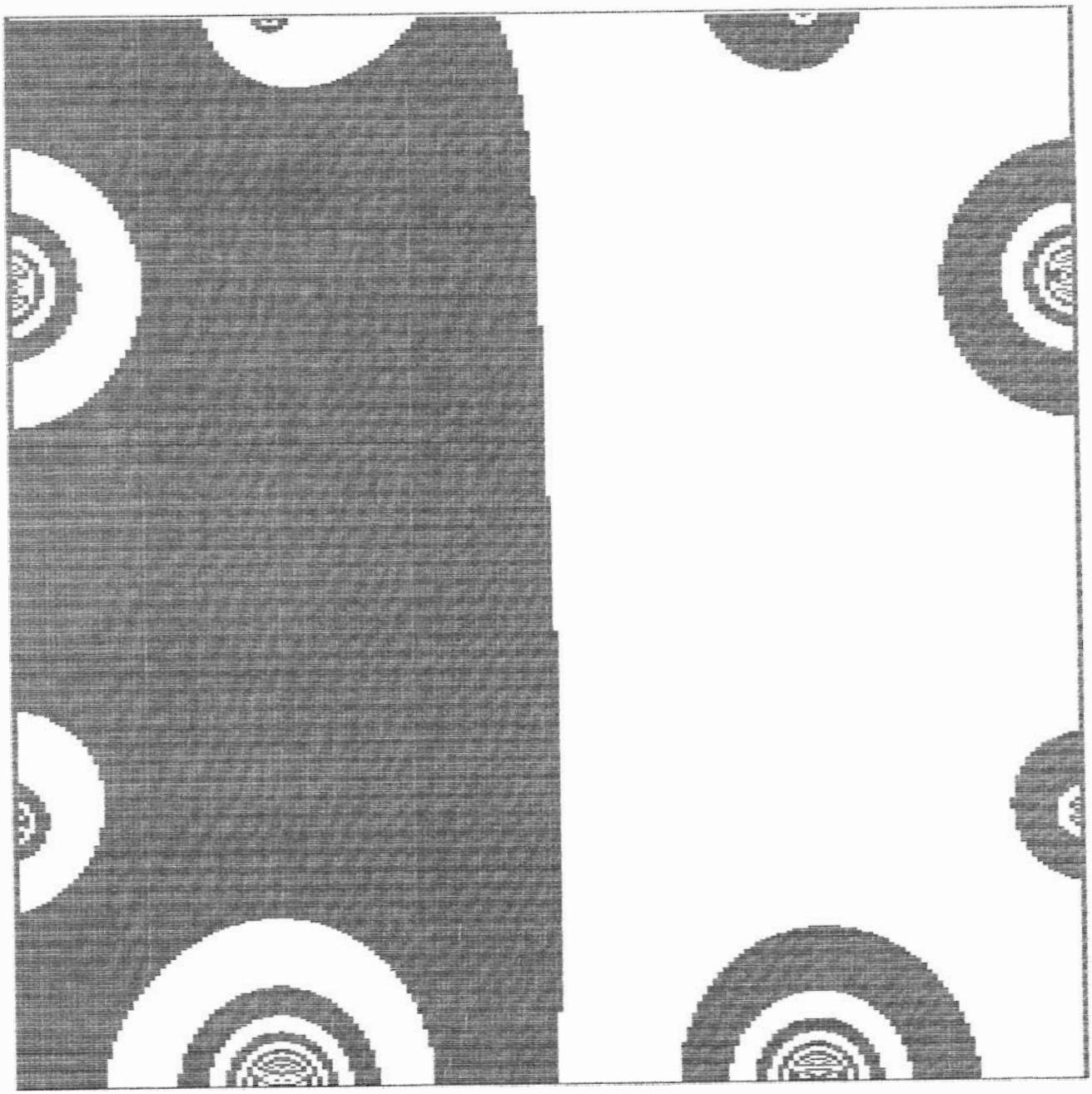

Figure 11. Magnetic scalar potential of error field in the plane of the poloidal gap of Tokapole II after correction (t = 0, no plasma).

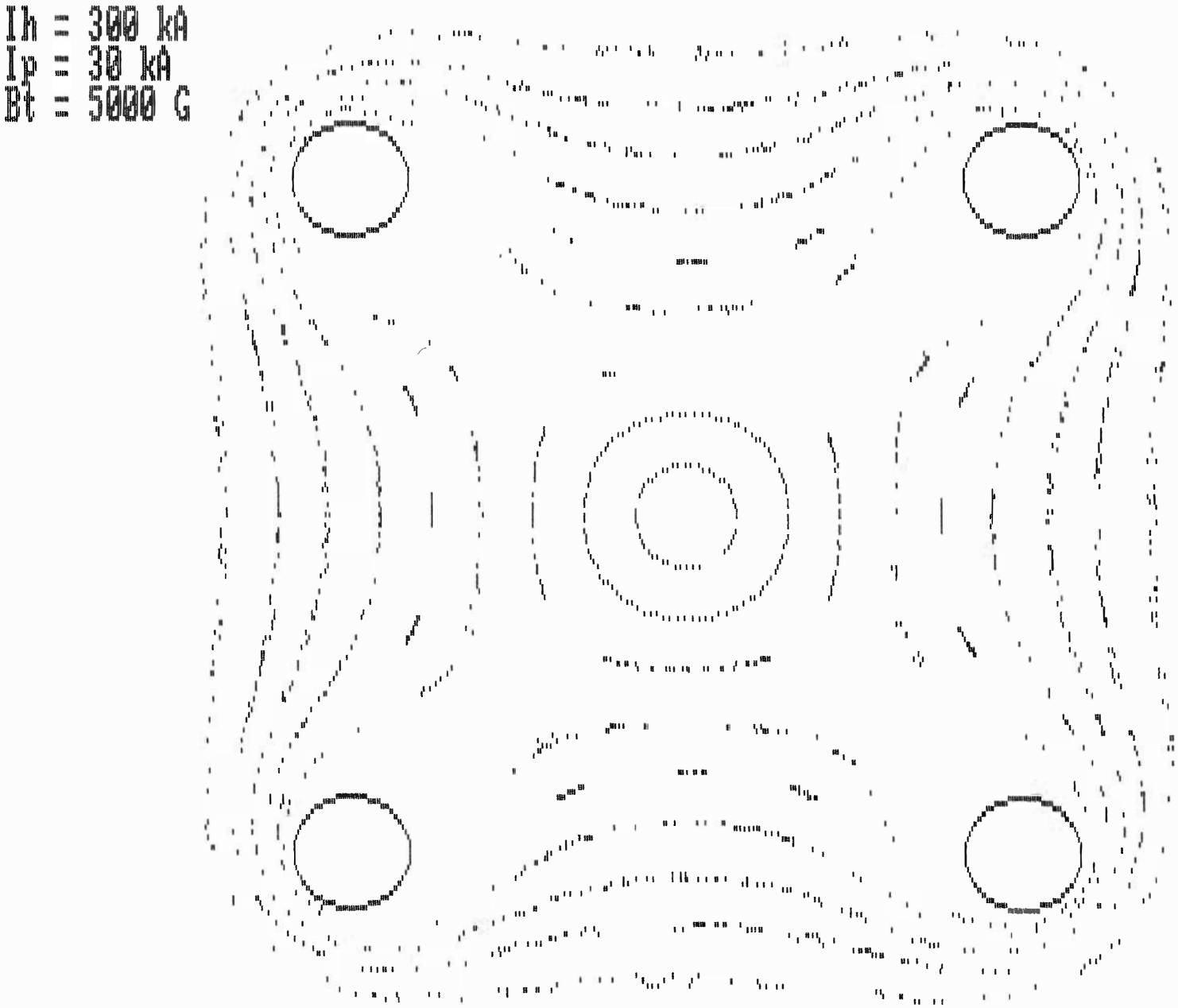

Figure 12. Poloidal puncture plot for Tokapole II after correction (with plasma).

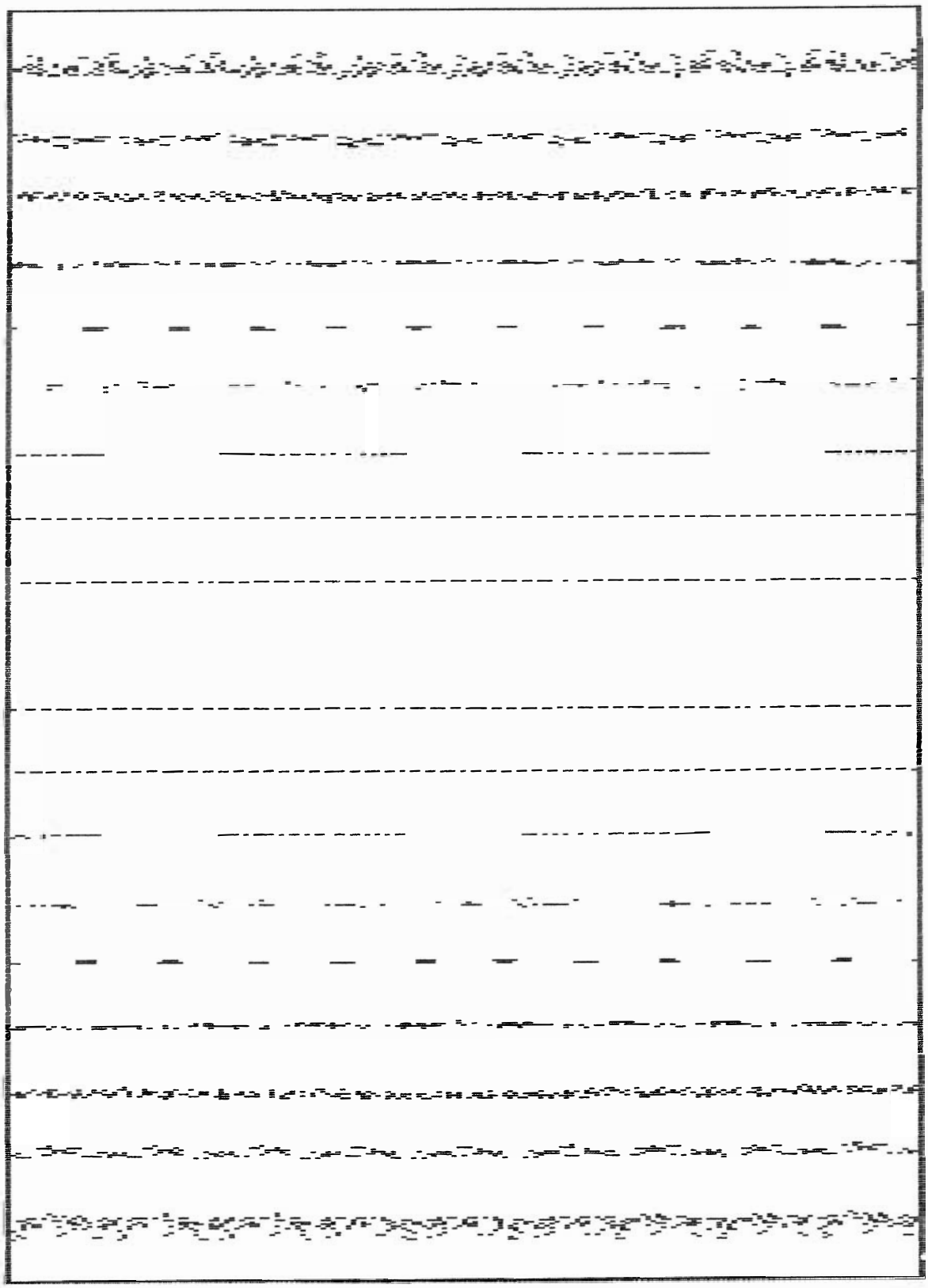

Figure 13. Toroidal puncture plot for Tokapole II after correction (with plasma).

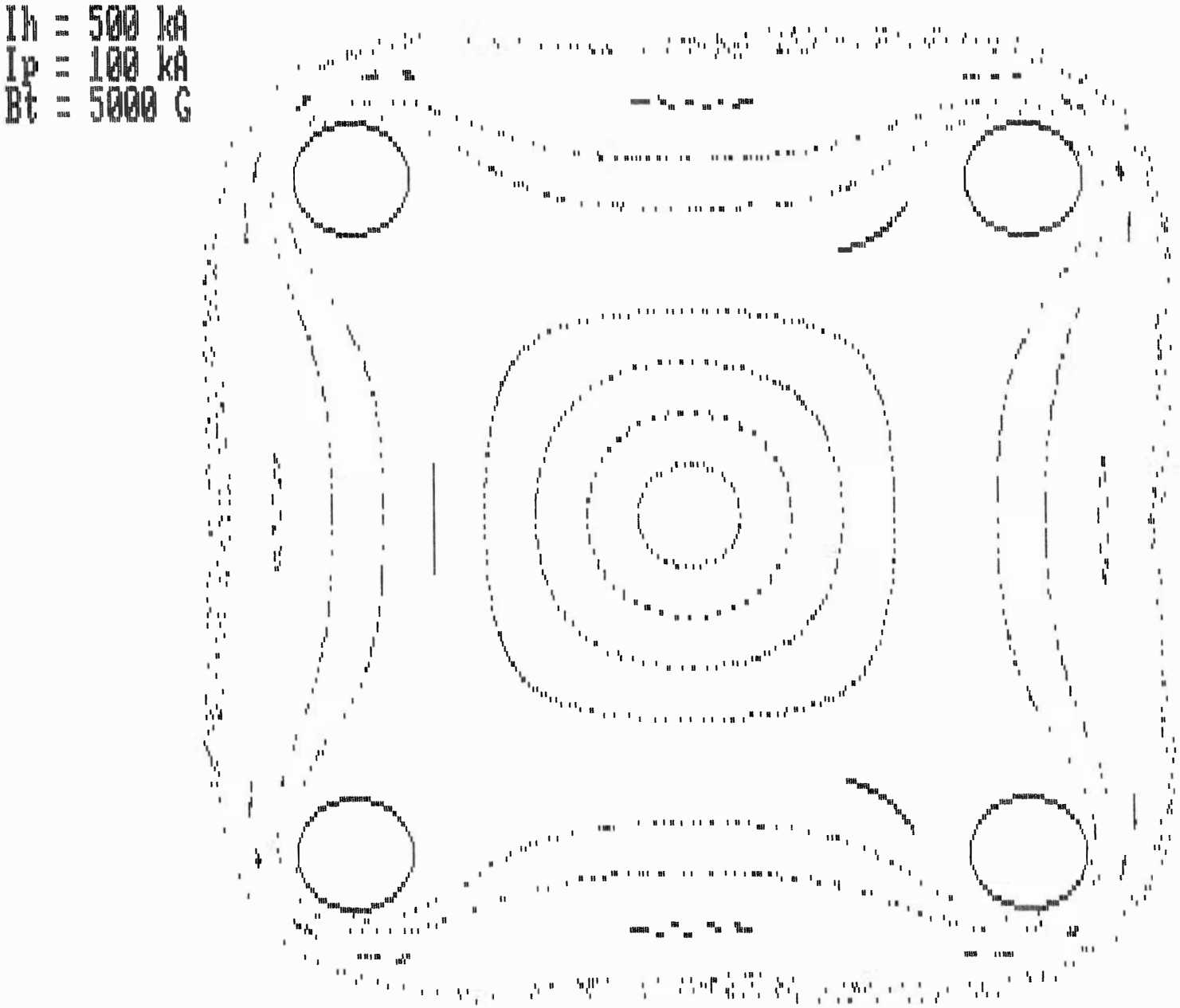

Figure 14. Poloidal puncture plot for Tokapole II after correction at current limit (with plasma).

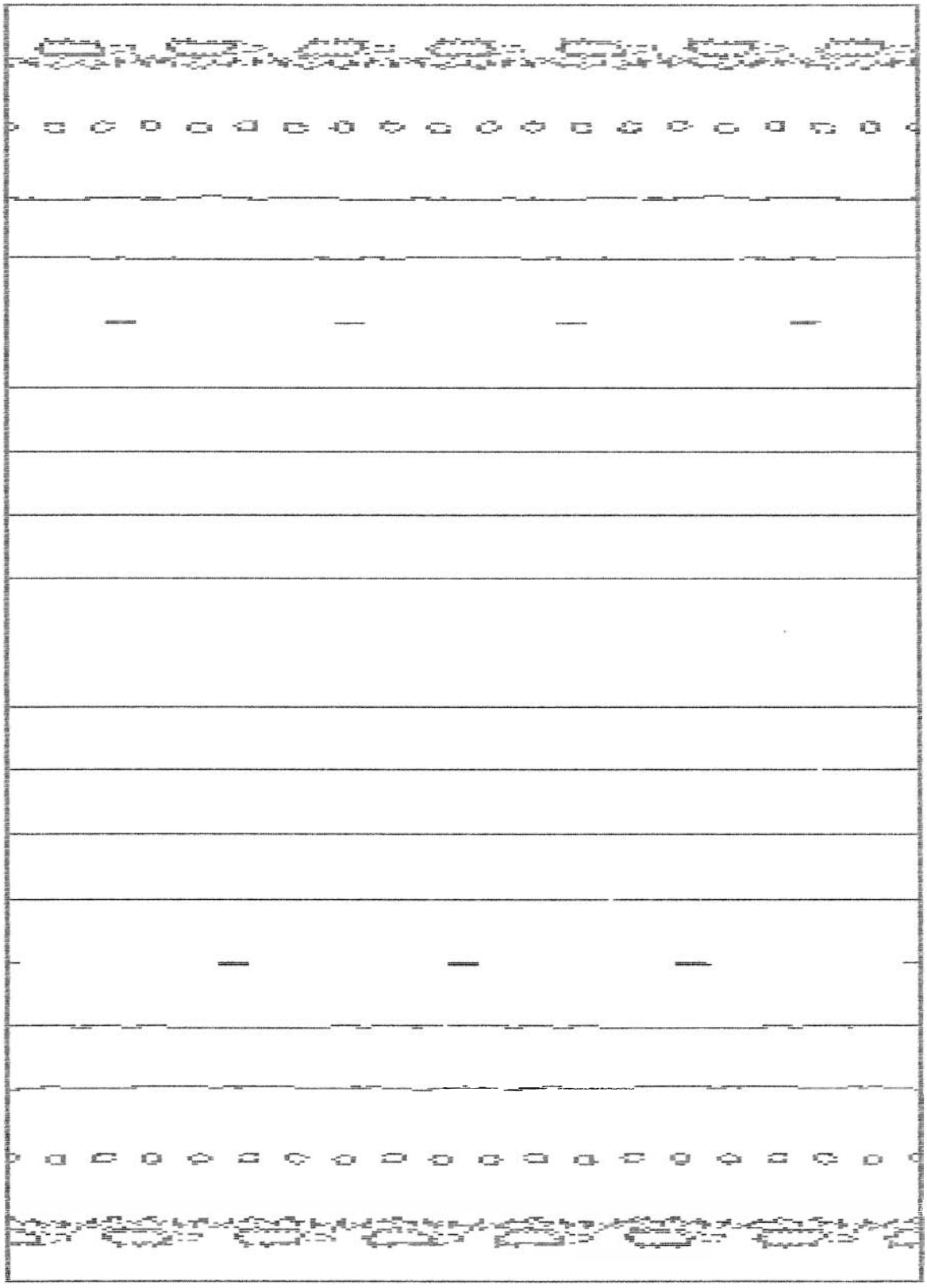

Figure 15. Toroidal puncture plot for Tokapole II after correction at current limit (with plasma).

field errors) for I_h/I_p = 310 kA / 170 kA is shown in figure 16. Except for the absence of noses and gussets, the flux plot resembles the experimental one.

First, a tokamak case was examined. A typical case is shot 350 from 14-May-1987. Data were taken at 3 ms, near the time of peak plasma current. Using the measured poloidal gap errors in the presence of plasma and the measured hoop current (310 kA), plasma current (170 kA, current density proportional to 1/r) and toroidal field (700 G, constant in space), the puncture plot of figure 17 was generated. Some good flux surfaces are evident near the axis, but otherwise the flux plot is quite stochastic.

In order to model an RFP case, some prescription for the spatial variation of the toroidal magnetic field is required. In a cylinder, we require $dB_t/dr = 0$ at r=0 and r=a, and $B_t(a) = F\langle B_t\rangle$, where F is the field reversal parameter and $\langle B_t\rangle$ is the value of B_t averaged over the circular cross section out to a radius r=a. If we further require that B_t be independent of r for F=1 (tokamak limit), the simplest polynomial expansion of $B_t(r)$ that satisfies all the requirements is

$$B_t(r) = [3 - 2F - 6(1-F)(r/a)^2 + 3(1-F)(r/a)^4]\langle B_t\rangle$$

Figure 18 shows a plot of $B_t(r)$ for a typical RFP case with $\langle B_t\rangle$ = 300 G and B_t = -100 G (F = -1/3). This is a reasonable representation of the toroidal field in an RFP and gives a

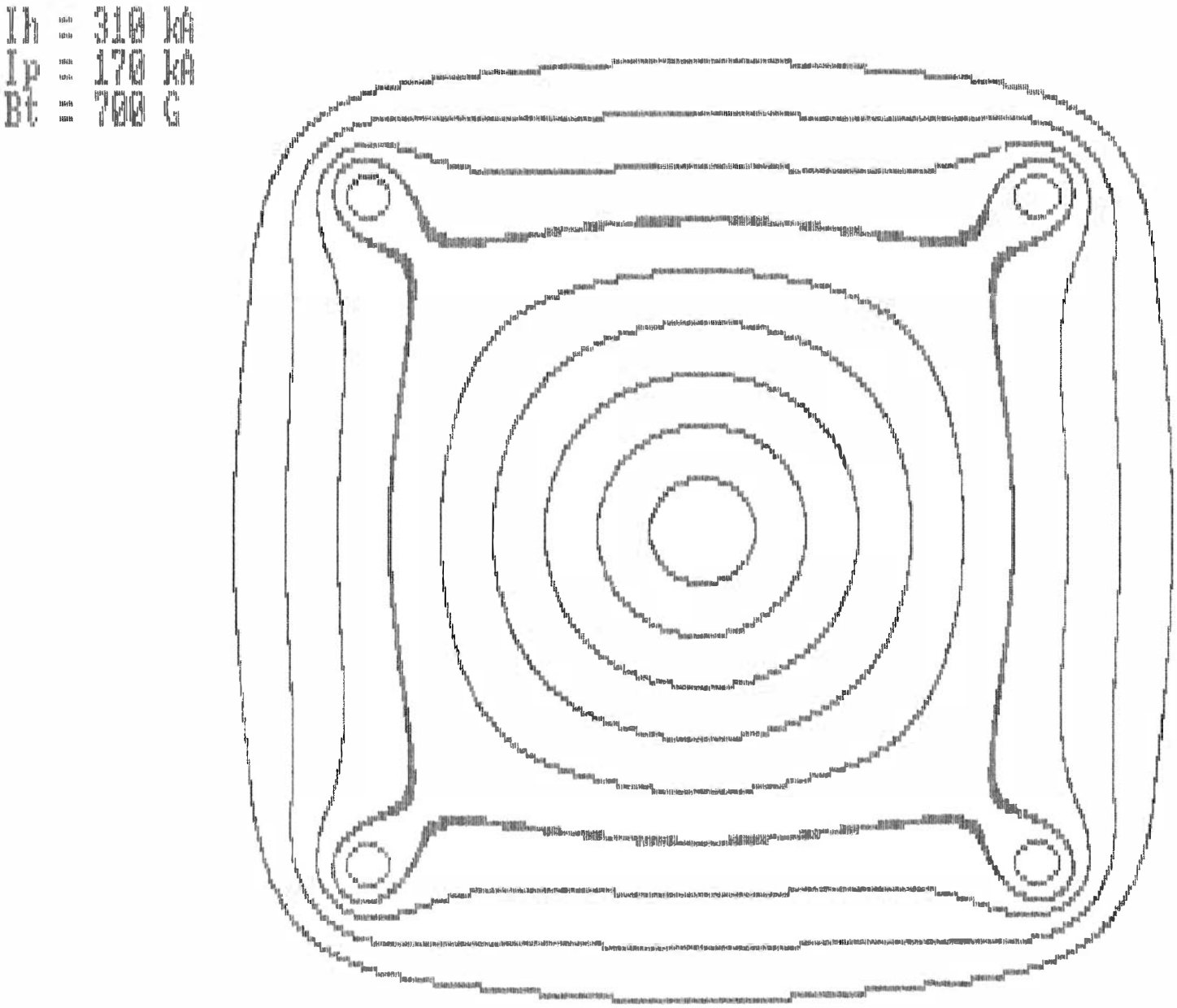

Figure 16. Equilibrium field flux plot used to model Poloidal Divertor RFP with J proportional to 1/r (no errors, with plasma).

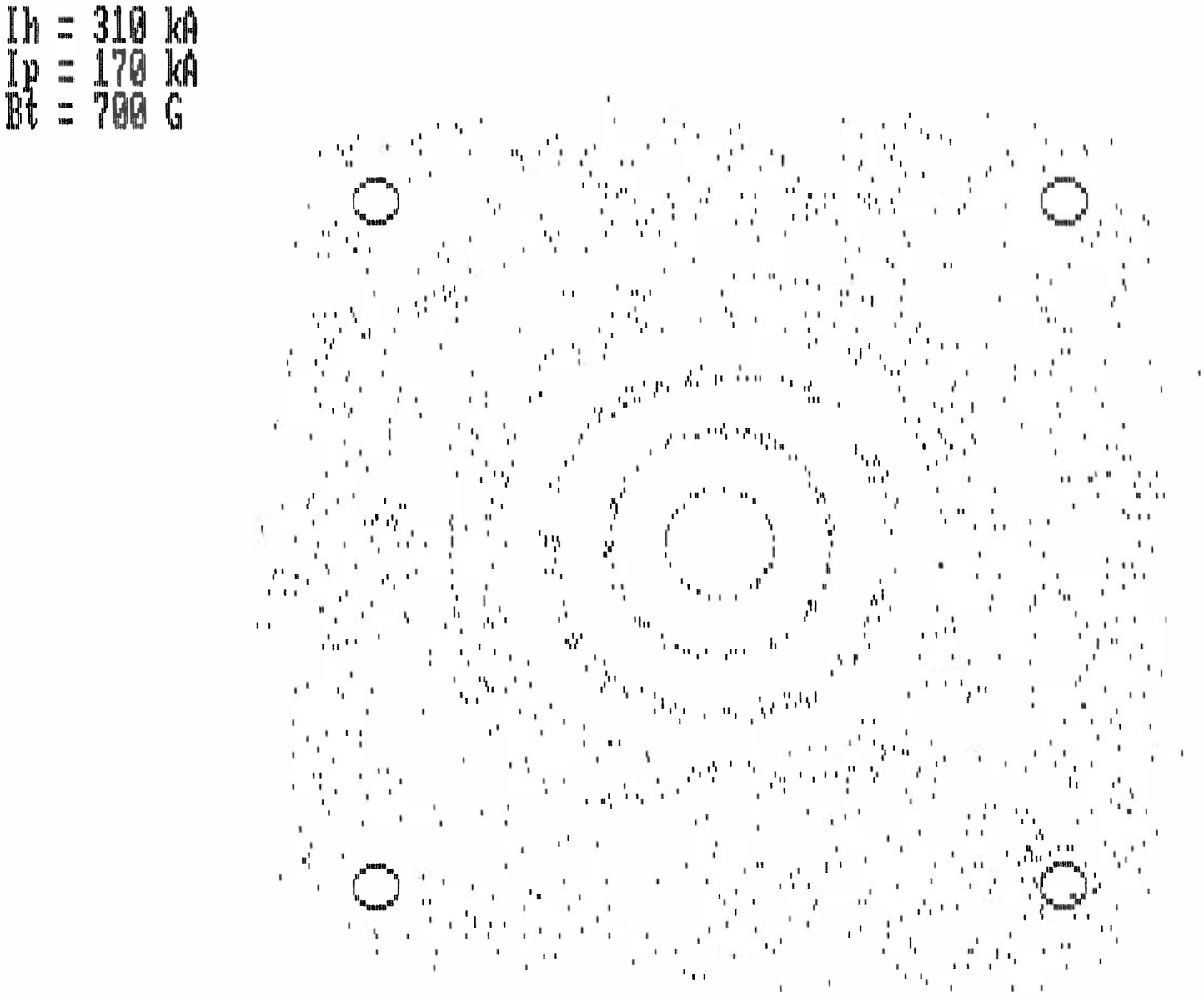

Figure 17. Poloidal puncture plot for Poloidal Divertor RFP (tokamak mode, with plasma).

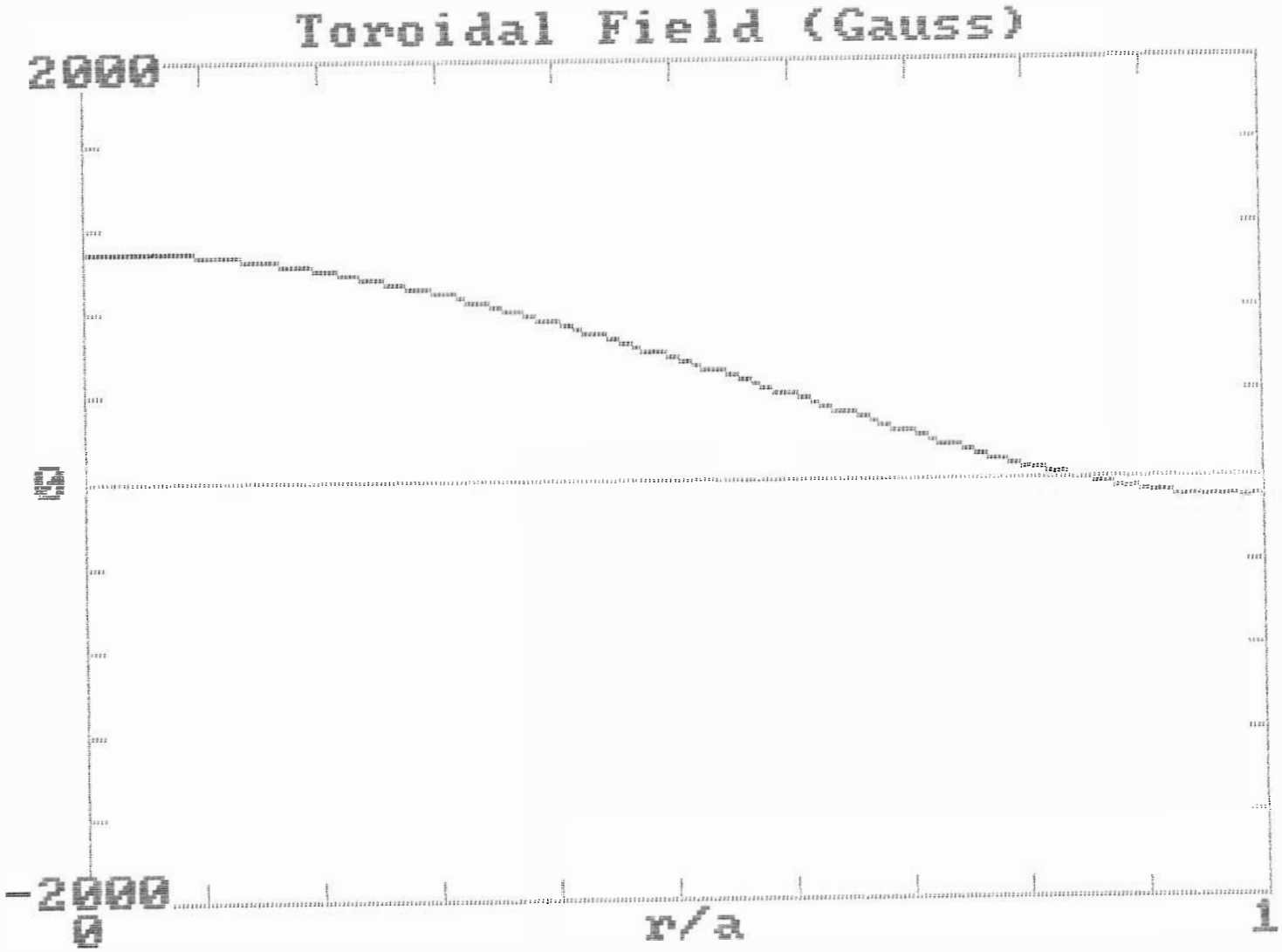

Figure 18. Toroidal field profile used to model Poloidal Divertor RFP (no errors, with plasma).

reversal surface at

$$r_R = \{1 - [F/3(F-1)]^{1/2}\}^{1/2} a$$

or about $r_R/a = 0.84$ for $F = -1/3$.

In order to represent the toroidal field in the noncircular RFP with internal rings, the above B_t profile was used in the midplane, and it was assumed that B_t is otherwise constant on a flux surface. In general this results in a reversal surface between the separatrix and the wall. In the presence of a field error, the field line wanders off the unperturbed flux surface, and thus the unperturbed toroidal field is not quite constant along the trajectory of the field line. This effect was ignored, but the variation of B_t along the trajectory of the field line as a result of the toroidal field of the error itself is included. The plasma current is assumed toroidal with a current density proportional to $1/r$ as with the tokamak case. Thus $\lambda = J/B$ is not particularly constant, but for the present purpose it is probably reasonably representative of the experimental situation.

The case calculated was shot 428 from 15-May-1987. Data were taken at 2 ms, near the time of maximum field reversal. Using the measured poloidal gap errors in the presence of plasma and the measured hoop current (240 kA), plasma current (135 kA), average toroidal field (300 G), and field at the wall (-100 G),

the puncture plot of figure 19 was generated. As for the tokamak case, the flux surfaces are good near the axis but completely stochastic near the edge. The good behavior near the axis is a result of the strongly peaked current density that gives a low q and high shear. The field errors for this case are sufficiently large that essentially all the field lines outside the separatrix exit through the poloidal gap within a few toroidal transits.

An alternate current profile is one for which $\lambda = J/B$ is constant. From $\nabla \times \underline{B} = \mu_o \underline{J}$ in the cylindrical approximation, the contribution to the poloidal field produced by the plasma corresponding to the previously described toroidal field profile is

$$B_\theta = \mu_o I_p r[3 - 2F - 3(1-F)(r/a)^2 + (1+F)(r/a)^4]/2\pi a^2$$

In order to apply this result to the noncircular case with internal rings, the poloidal field is calculated in the midplane and assumed constant in magnitude along the trajectory of a field line. The equilibrium flux plot corresponding to this case is shown in figure 20 and is practically indistinguishable from the case with J proportional to 1/r.

Applying the experimentally measured poloidal gap errors to this relatively weakly sheared equilibrium (q=0.2 on axis) results in a puncture plot with virtually no closed flux surfaces and field lines that leave the poloidal gap in only a few toroidal transits. It is hardly surprising that sustained RFP

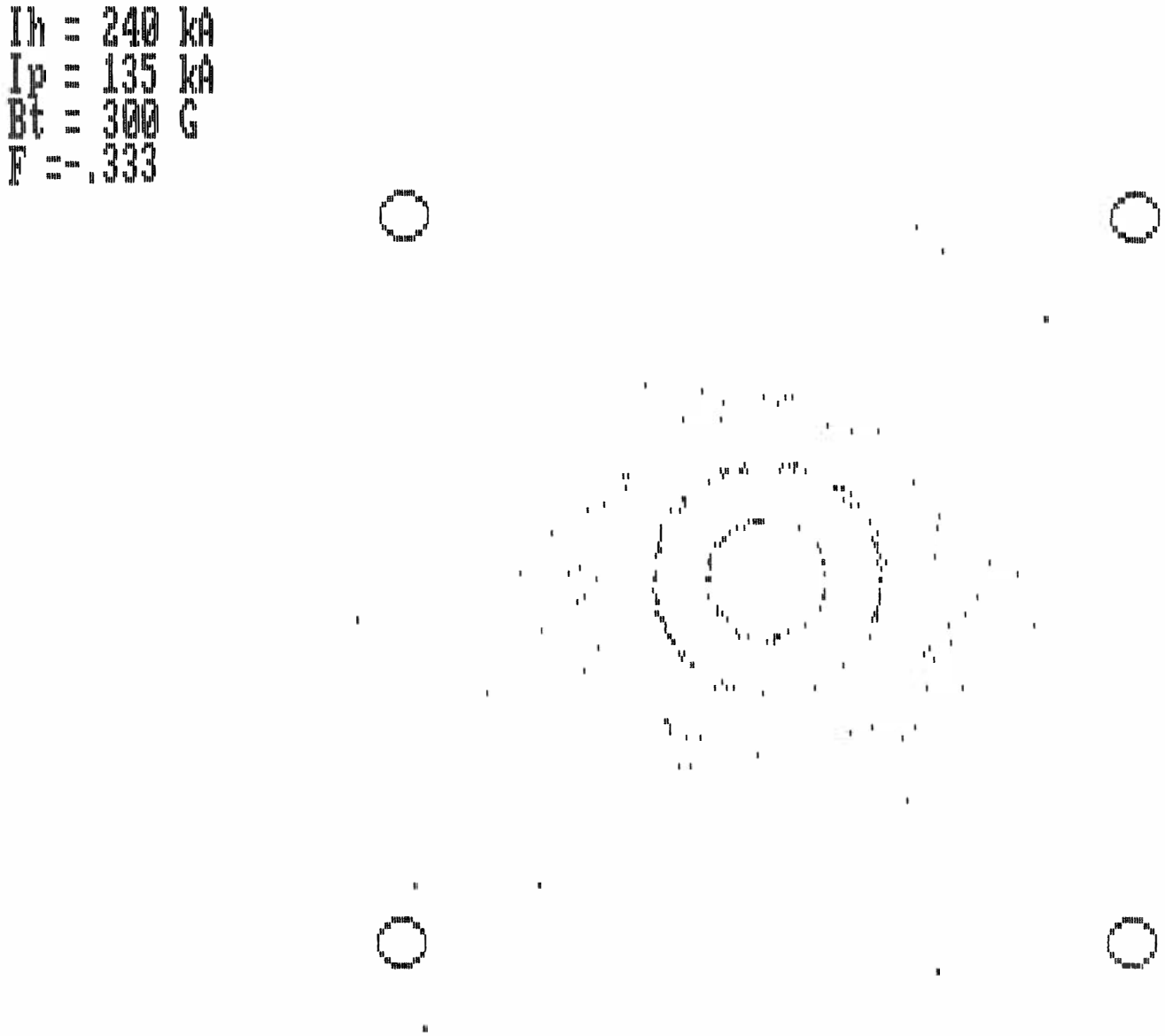

Figure 19. Poloidal puncture plot for Poloidal Divertor RFP (RFP mode, with plasma).

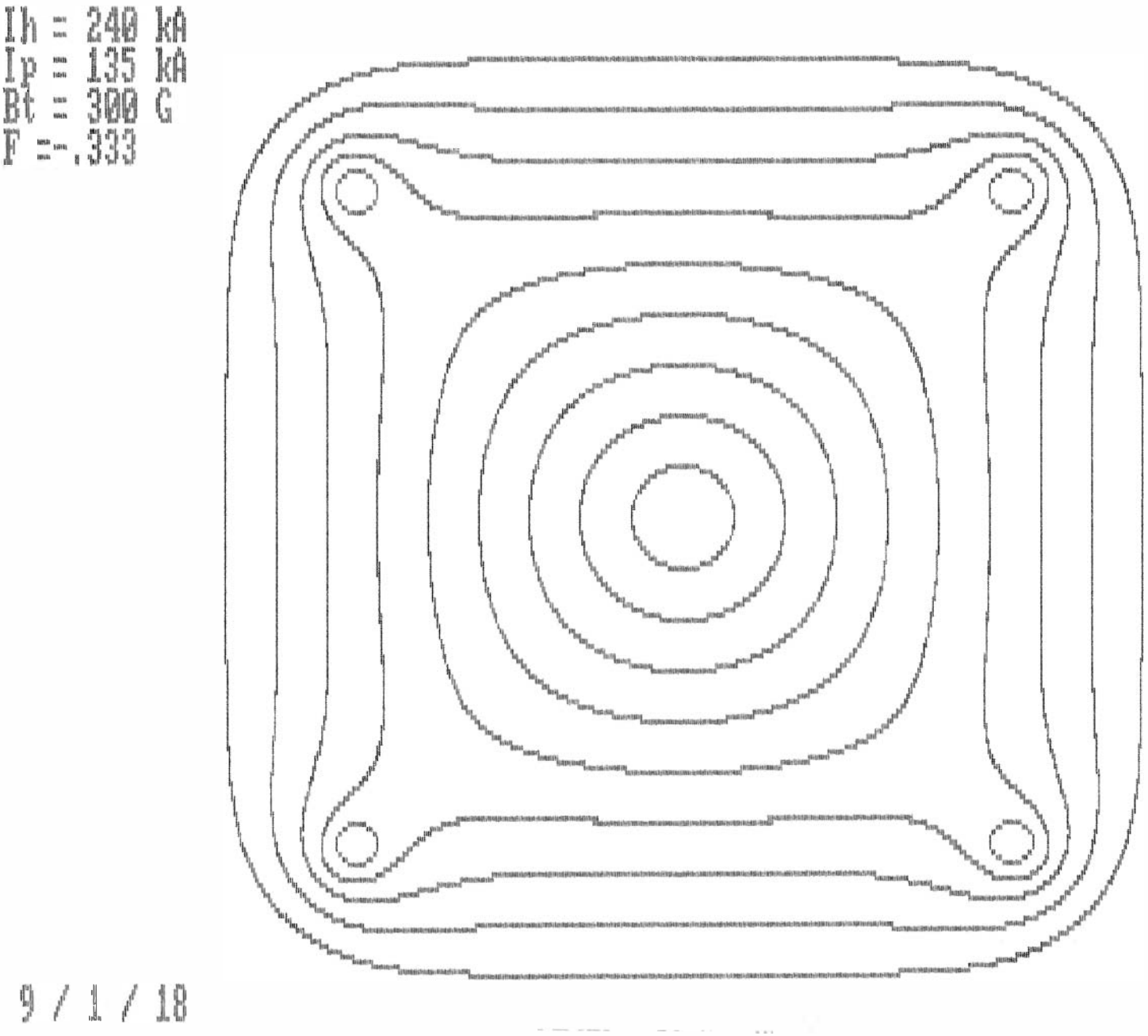

Figure 20. Equilibrium field flux plot used to model Poloidal Divertor RFP with λ=const (no errors, with plasma).

discharges could not be obtained under these conditions. The machine was decommissioned before a serious attempt could be made to reduce the errors. Further experimental studies of the effect of gap errors on RFP plasmas must await the delivery and installation of MST.

V. Gap Error Correction Schemes

The most obvious way to avoid a gap error is to arrange for the windings that drive the gap to cross the gap with the proper distribution to match the current density in the wall far from the gap. Good practice dictates that this be done as accurately as possible, but it can never be perfect. Even if one could calculate the desired distribution with absolute accuracy, changing plasma conditions and other time-dependent effects such as soak-in would generate errors.

One possibility that offers some advantage is to connect some of the windings in parallel rather than in series. Then when more current is demanded from one portion of the gap, the winding current automatically readjusts in a way that is not possible when the windings are in series. If the machine has an inherent symmetry (such as up/down) and an inherent asymmetry (such as in/out), it is best to parallel turns on the asymmetric sides rather than the symmetric sides. Thus if the poloidal field windings are split into two parallel bundles, the split should be at the midcylinder rather than at the midplane.

Parallel windings also allow easy trimming by adding a small series impedance in one or more of the bundles of turns. Varying the resistance and reactance of this impedance provides some control of the time-dependence of the error. Windings in series can also be trimmed with a shunt element, but it must have a high

impedance, and thus is inherently difficult using inductors. One could use a series RC in parallel with a series winding bundle, but the possibility of resonances makes the time-dependence somewhat more complex.

Another cure is the use of a long flange connected to the gap (see PLP 965). The flange has the effect of placing the windings far from the region where a field error would cause harm. The flange allows the current streamlines to gradually readjust along its length. However, the current density in the flange is determined at early times by its inductance (primarily the gap spacing) and at late times by its resistance (thickness). Thus a poorly designed flange may do more harm than good. Usually space limitations restrict the length of the flange. The flange may be folded, however. The current distribution in the flange can be adjusted by varying the gap spacing and/or the resistivity by, for example, drilling in the flange holes that can be selectively filled with conducting plugs. In practice, such holes are capable of correcting only relatively minor errors.

Just as the radial flux emerging from the gap provides a measure of the field error, any scheme that reduces the radial flux also reduces the error. Thus a conducting plate placed over the gap eliminates the error, at least on the time scale of the field soaking into the plate. Such a shield is topologically similar to a folded flange except that it need not be connected

to the wall of the machine. Its purpose is to generate eddy currents which produce a radial flux that cancels the radial flux of the error. The eddy currents can also be viewed as transposing the driving currents from where they are to where they should be.

If it is inconvenient to shield the gap with a continuous plate, discrete current loops can be used instead. The numerology for correcting errors with such loops is the same as for measuring errors. For example, eight loops can eliminate m=0 through m=3 and one phase of m=4, subject to considerations of aliasing with higher harmonics as described earlier. In the case of discrete loops, it is difficult to make them passive because their L/R time is typically small compared to the duration of the pulse that they are designed to correct. Perhaps soon new high-temperature superconductors appropriate for the task will be available. Meanwhile, one must typically drive them with some external current. To the extent that the field error has the same time-dependence as the field produced by the gap voltage, the correction coils can be connected in series with the main windings, perhaps with some kind of current transformer to provide the correct magnitude of current. One could also drive them in parallel with the main windings if care is taken to adjust their inductance and resistance appropriately to get a reasonably correct time-dependence, but this is difficult because the inductance and resistance of the plasma are typically complicated functions of time and experimental conditions.

Correction coils driven either in series of parallel with the main windings are capable of correcting only a particular plasma current profile and cannot in general accomodate to changing plasma conditions.

A possible solution is to sense the radial error field and then to apply feedback through high-gain amplifiers to coils whose purpose is to drive the error field to zero (see the DOE proposal for Reversed Field Pinch Studies, February, 1984). In this way, the effective L/R time of each coil is multiplied by the gain of its amplifier. Practical applications of this idea are limited by the availability of amplifier components with sufficient power and speed and by the usual problems of linearity, efficiency, phase shifts, stability, etc. Such a solution would be very eligent, however, since it can compensate for all time-dependent effects and changing plasma conditions.

If the error field is spatially Fourier transformed as described in the previous sections, it is likely that the largest errors have low mode numbers (m = 0,1,2,etc.). Furthermore, the low mode errors are typically most detrimental because they penetrate more deeply into the region containing the plasma and often more easily resonate with helical field lines inside the plasma. Thus the method of attacking field errors is normally to work first on the lowest mode and to worry about higher mode numbers only after the lower ones have been eliminated.

In this connection, it is useful to note that each mode, with the exception of m=0, requires two independent adjustments to eliminate. These can be thought of as amplitude and phase, sine and cosine, horizontal and vertical or some combination. To eliminate m=0 through m=4 thus requires a total of nine independent adjustments and even then one can be assured that the correction is perfect only at one particular time during the pulse. Ideally the adjustments should each encompass a separate adjustment for the resistive and reactive components so that one can eliminate the error at two times, typically very early in the pulse and very late. The hope then would be that the error is acceptably small at intermediate times. Alternately one can pick a time in the middle of the pulse at which the field error is made zero and then use the other adjustment to minimize the rate of change of field error near the time of interest.

Actually, the situation is not quite as complicated as described above since the m=0 error is often generated as a consequence of the higher errors and disappears automatically when the others are eliminated. Furthermore, there are often inherent symmetries in the machine (up/down) that dictate the phase of the higher modes. Finally, for many cases, the time-dependence is relatively weak. Thus in practice four independent adjustments usually suffice to reduce the modes through m=4 to an acceptably low value.

Appendix A

```
'Program PUNCTURE.BAS
'This Turbo BASIC program follows a field line in a
'large aspect ratio representation of Tokapole II,
'and plots on the screen the poloidal location of
'the field line every time it punctures a particular
'toroidal azimuth or the radial location everytime it
'punctures the midplane.
cls
screen 2
dim x(8),y(8),z(8),S(8)
R=.5 'major radius of machine in m
a=.22 'half height of machine in m
h=.145 'hoop distance from midplane in m
rh=.025 'hoop minor radius in m
Ih=300000 'hoop current in amps
Ip=30000 'plasma current in amps
Bt=.5 'average toroidal field in tesla
F=1 'field reversal parameter (1 for tokamak)
Lo=2.2e-7 'machine inductance in Henrys
Nc=10 'number of contour lines
Nt=50 'number of toroidal transits
dl=.005 'step size in m
p%=0 '0 for x-y plot, 1 for x-z plot
pi=3.1415926536
mu=4*pi*1.0e-7
kh=mu*Ih/8/pi
kp=mu*Ip/a/pi
L=2*pi*R
for k=1 to 8 'monopoles represent gap error
        read x(k),y(k),z(k),S(k)
        z(k)=z(k)*L
        S(k)=S(k)*Lo*Ih/4/pi/38000
next k
data  .22, .11, .5,  5
data  .11, .22, .5,-34
data -.11, .22, .5, 13
data -.22, .11, .5,-52
data -.22,-.11, .5, 46
data -.11,-.22, .5, -8
data  .11,-.22, .5, 33
data  .22,-.11, .5, -4
print"Ih =";Ih/1000;"kA"
print"Ip =";Ip/1000;"kA"
print"Bt =";int(1e4*Bt+.5);"G"
print"F =";int(1000*F+.5)/1000
circle(240*h/a+320,100-100*h/a),240*rh/a
circle(240*h/a+320,100+100*h/a),240*rh/a
circle(-240*h/a+320,100-100*h/a),240*rh/a
circle(-240*h/a+320,100+100*h/a),240*rh/a
h=h+0.12*rh*(1+5*Ip/Ih)
if p%=1 then cls: line(20,10)-(620,190),1,B
for i=1 to Nc-1
        x=-a*i/Nc: dx=0
```

```
        y=0: dy=0
        z=L: dz=0
        Btr=Bt*(3-2*F-6*(1-F)*(x/a)^2+3*(1-F)*(x/a)^4)
        gosub 10
        def seg = &HB800
        bsave"puncture.dat",0,&H4000
next i
while inkey$<>chr$(27): wend
cls
end
10 'follow field lines
for j=1 to Nt*i
        locate 25,1
        print i;"/";j-1;"/";Nt*i;" ";
        while z<L
                xo=x: yo=y: zo=z: gosub 20
                dx1=dl*Bx/B: dy1=dl*By/B: dz1=dl*Bz/B
                x=xo+dx1/2: y=yo+dy1/2: z=zo+dz1/2: gosub 20
                dx2=dl*Bx/B: dy2=dl*By/B: dz2=dl*Bz/B
                x=xo+dx2/2: y=yo+dy2/2: z=zo+dz2/2: gosub 20
                dx3=dl*Bx/B: dy3=dl*By/B: dz3=dl*Bz/B
                x=xo+dx3: y=yo+dy3: z=zo+dz3: gosub 20
                dx4=dl*Bx/B: dy4=dl*By/B: dz4=dl*Bz/B
                x=xo+(dx1+2*dx2+2*dx3+dx4)/6
                y=yo+(dy1+2*dy2+2*dy3+dy4)/6
                z=zo+(dz1+2*dz2+2*dz3+dz4)/6
                if p%=1 then if y*yo<=0 then gosub 40
                if inkey$=chr$(27) then cls: end
        wend
        if p%=0 then gosub 50
        z=z-L
next j
locate 25,1
print string$(14,32);
return
20 'calculate fields
        r=sqr(x*x+y*y)
        xl=x-h: xg=x+h:yl=y-h: yg=y+h
        xl2=xl*xl: xg2=xg*xg: yl2=yl*yl: yg2=yg*yg
        Bx=yl/(xl2+yl2)+yl/(xg2+yl2)+yg/(xl2+yg2)+yg/(xg2+yg2)
        Bx=kh*Bx+kp*y/r
        By=xl/(xl2+yl2)+xl/(xl2+yg2)+xg/(xg2+yl2)+xg/(xg2+yg2)
        By=-kh*By-kp*x/r
        Bz=Btr: gosub 30
        B=sqr(Bx*Bx+By*By+Bz*Bz)
return
30 'add field error
for k=1 to 8
        xk=x-x(k): yk=y-y(k): zk=z-z(k)
        r3=xk*xk+yk*yk+zk*zk: r3=S(k)/sqr(r3*r3*r3)
        Bx=Bx-xk*r3
        By=By-yk*r3
        Bz=Bz-zk*r3
next k
return
```

```
40 'plot x-z contour
        xp=xo-yo*(x-xo)/(y-yo)
        zp=zo-yo*(z-zo)/(y-yo)
        pset(300*xp/a+320,190-180*zp/L)
return
50 'plot x-y contour
        xp=xo-(zo-L)*(x-xo)/(z-zo)
        yp=yo-(zo-L)*(y-yo)/(z-zo)
        pset(240*x/a+320,100-100*y/a)
return
```